Article

A probiotic *Limosilactobacillus fermentum* GR-3 mitigates colitis-associated tumorigenesis in mice via modulating gut microbiome

Check for updates

Tuoyu Zhou[1,2,8], Jingyuan Wu[3,8], Aman Khan[1], Tianxiang Hu[4], Yiqing Wang[3], El-Sayed Salama[5], Shaochen Su[6], Huawen Han[2] ✉, Weilin Jin[7] ✉ & Xiangkai Li [1] ✉

Bacterial therapy for colorectal cancer (CRC) represents a burgeoning frontier. The probiotic *Limosilactobacillus fermentum* GR-3, derived from traditional food "Jiangshui", exhibited superior antioxidant capacity by producing indole derivatives ICA and IPA. In an AOM/DSS-induced CRC mouse model, GR-3 treatment alleviated weight loss, colon shortening, rectal bleeding and intestinal barrier disruption by reducing oxidative stress and inflammation. GR-3 colonization in distant colon induced apoptosis and reduced tumor incidence by 51.2%, outperforming the control strain and vitamin C. The beneficial effect of GR-3 on CRC was associated with gut microbiome modulation, increasing SCFA producer *Lachnospiraceae* NK4A136 group and suppressing pro-inflammatory strain *Bacteroides*. Metagenomic and metabolic analyses revealed that GR-3 intervention upregulated antioxidant genes (*xseA*, *ALDH*) and butyrate synthesis gene (*bcd*), while increasing beneficial metabolites (SCFAs, ICA, IPA, VB12 and VD3) and reducing harmful secondary bile acids. Overall, GR-3 emerges as a promising candidate in CRC therapy, offering effective gut microbiome remediation.

Colorectal cancer (CRC) stands as the second leading cause of cancer-related mortality, with a notable increase in global cases, reaching an incidence rate of 19.5 per 100,000 individuals in 2020[1]. This significant upsurge can be attributed to various factors, including shifts in dietary patterns (e.g. high intake of red meats and low intake of fiber), a rise in sedentary lifestyles, and genetic predispositions[2]. The predominant treatment modalities for CRC include surgery, radiotherapy, and chemotherapy[3]. However, these treatments possess their own drawbacks. For example, surgery has strict requirements for the patient's physical condition, and is not suitable for advanced or metastatic tumors[4]. Radiotherapy, while advantageous alongside surgery or for palliative purposes, might lead to enduring complications like bowel dysfunction[5]. Chemotherapy affects both healthy and malignant cells due to its lack of targeting specificity[6], resulting in a spectrum of systemic side effects, from mild nausea to profound myelosuppression[7].

This underscores the pressing need for more effective CRC therapeutic strategies, among which probiotic therapy is considered a promising new approach.

Various probiotic strains have been employed for CRC treatment. Bender et al. discovered that *Lactobacillus reuteri* can stimulate cytotoxicity of CD8 + T cells to melanoma by secreting indole-3-aldehyde[8]. *Lactobacillus gallinarum* modulates the gut microbiota and produces indole-3-lactic acid to inhibited intestinal tumorigenesis[9]. *Streptococcus thermophilus* inhibits colorectal tumorigenesis by secreting β-galactosidase[10]. However, the colonization efficiency of these natural probiotics in the gut is merely 0.5% to 1%, indicating that the inherent capabilities of probiotics may be insufficient for CRC treatment[11–13]. Existing evidences highlighted the role of probiotics in regulating intestinal microbiota and maintaining intestinal homeostasis[14]. For example, *Pediococcus acidilactici* BT36, which lacks the

[1]Ministry of Education Key Laboratory of Cell Activities and Stress Adaptations, School of Life Sciences, Lanzhou University, Lanzhou, Gansu, 730000, China. [2]State Key Laboratory of Grassland Agro-ecosystems, College of Pastoral Agricultural Science and Technology, Lanzhou University, Lanzhou, China. [3]The First Clinical Medical College of Lanzhou University, Lanzhou University, Lanzhou, 730000, China. [4]Georgia Cancer Center, Augusta University, 1410 Laney Walker Blvd, Augusta, GA, 30912, USA. [5]Department of Occupational and Environmental Health, School of Public Health, Lanzhou University, Lanzhou, 730000 Gansu Province, PR China. [6]Healthy Examination & Management Center, First Hospital of Lanzhou University, Lanzhou, 730000, China. [7]Medical Frontier Innovation Research Center, The First Hospital of Lanzhou University, Lanzhou, China. [8]These authors contributed equally: Tuoyu Zhou, Jingyuan Wu.
✉e-mail: hanhuawen@lzu.edu.cn; ldyy_jinwl@lzu.edu.cn; xkli@lzu.edu.cn

ability to reduce hexavalent chromium, modulated the gut microbiota to counteract Cr (VI) toxicity[11]. Butyrate-producing *Clostridium* spore wrapped in fructo-oligosaccharide can regulate the gut microbiota to suppress CRC by increasing the abundance of SCFAs-producer[15]. Moreover, fecal microbiota transplantation can counteract the dysbiosis of the gut microbiome, with subsequently inhibiting tumor proliferation[16].

Redox status is a potential determinant of overall health[17]. Oxidative stress, resulting from an imbalance in redox homeostasis, has been implicated in the development of various diseases, including cardiovascular diseases, cancer, and neurodegenerative disorders[18,19]. Antioxidants play a crucial role in modulating redox homeostasis[20]. By maintaining the balance between oxidation and reduction reactions, antioxidants contribute to preserve cellular function and integrity[21,22]. Vitamin C (VC) exhibited inhibitory effects on the growth and proliferation of CRC[23]. However, its specific mechanism remains unclear. CRC patients often manifest gut microbial dysbiosis, characterized by an upsurge in opportunistic pathogens and harmful metabolites[24]. Disrupted gut microbiota can also lead to oxidative stress[25]. For instance, *E. faecalis* produced hydroxyl radicals, contributing to genomic instability in CRC[26]. Gut microbiota-derived deoxycholic acid derived has been linked to oxidative damage and higher CRC risk in peroxide-induced rat tumor models[27]. Cancer cells consistently experience oxidative stress, evident from the increased reactive oxygen species within the tumor microenvironment[28]. Thus, the antioxidant properties of VC may be the potential mechanisms for preventing tumor development. Probiotics not only exhibit antioxidant capabilities but can also effectively modulate the gut microbiota[29]. Previous studies on probiotics focused mainly on their anti-cancer metabolites, neglecting their antioxidant properties. We hypothesize that probiotics with strong antioxidant properties can combat CRC by reshaping the gut microbiota.

"Jiangshui", a traditional fermented food originating from the high-altitude regions of northwest China, has become a hotspot of research due to its abundant natural probiotics[30]. The high-altitude environment, characterized by intense ultraviolet radiation, naturally favor microbes with robust antioxidative traits[31]. Among the strains isolated from "Jiangshui", *Limmosilactobacillus fermentum* GR-3 demonstrates the highest antioxidant capabilities. This strain has been confirmed to promote uric acid degradation in both a hyperuricemic mouse model and human trials by modulating the gut microbiota[12,32]. Considering the role of gut microbiota dysbiosis and inflammation-induced oxidative stress in CRC progression[33,34], this study evaluated the attenuating effect of *L. fermentum* GR-3 on an AOM/DSS induced CRC mouse model. The evaluation encompassed analyses of intestinal barrier integrity, inflammatory factors expression, oxidative stress levels, tumor apoptosis pathways, and shifts in gut microbiome. Our findings may facilitate the application of *L. fermentum* GR-3 in CRC prevention and offer insights into devising safe and efficacious CRC treatment strategies.

Result

Probiotic *L. fermentum* GR-3 exhibited superior antioxidant capabilities in vitro

To identify the most suitable probiotic strain for CRC therapy, seven probiotics were chosen to evaluate their antioxidant capabilities in vitro. Strain GR-3 exhibited the highest overall antioxidant level (0.35 mM) and DPPH free radical scavenging activity (45.6%), which was about 2.8 times higher than that of *L. plantarum* J6 (Fig. 1A). In contrast, another "Jiangshui" probiotic strain GR-6 showed the maximum effect on monolayer tumor cells in vitro, reducing the activity of RKO and SW480 cells by 58% and 55%, respectively (Fig. 1B). Based on the phylogenetic tree analysis from 16S rRNA sequencing (Fig. 1C) and scanning electron microscopy images (Fig. 1D), strains GR-3 and GR-6 were identified as *L. fermentum* and *P. acidilactici*, respectively. The co-incubation of SW480 tumor cells with GR-3 or GR-6 observed obvious cell death and atrophy compared with CK group (Fig. 1E). Flow cytometry analysis indicated that the proportion of viable cancer cells from GR-3 and GR-6 treatment groups was 50.9% and 31.2%, respectively, lower than the control group (80.5%) (Fig. 1F). qRT-PCR

analysis further revealed that the elevated mRNA levels of p53 and Bax in CT26 cells treated by GR-3 and GR-6, while the Bcl-2 mRNA levels decreased (Fig. 1G). Compared to GR-6, GR-3 induced higher Bax expression in CT26 cells. In contrast, GR-6 more effectively downregulated β-catenin mRNA levels in CT26 cells (Fig. S1). Probiotic-mediated indole derivatives are associated with antitumor effects[8,9]. Non-target metabolite analysis showed that strains GR-3 and GR-6 can produce indole-3-carboxylic acid (ICA), indole-3-lactic acid (ILA), indole-3-acetic acid (IAA), and indole-3-propionic acid (IPA) (Fig. 1H). Strain GR-3 secreted more IPA than strain GR-6, while strain GR-6 produced higher levels of ICA and ILA. IAA production was identical between these two strains treatment group. These findings suggest that GR-3 and GR-6 could serve as effective probiotics for CRC treatment. Recognizing the potential importance of antioxidative capabilities in CRC therapy[35], GR-3 was selected for deeper investigation, with GR-6 serving as a control strain.

L. fermentum GR-3 ameliorated the AOM/DSS induced intestinal tumorigenesis, colon shortening and occult blood

The protective effects of probiotics against CRC triggered by AOM/DSS were examined and compared with the first-line anticancer drug 5-fluorouracil (5-FU) and the antioxidant Vitamin C (VC) (Fig. 2A). The qPCR analysis revealed the colonization frequencies of GR-3 and GR-6 ranged from 0.01% to 0.06% in gut milieu (Fig. S2). Each administration of DSS resulted in a decrease in probiotics abundance. While food intake remained consistent across all mouse groups (Fig. S3), the AOM/DSS-induced CRC mice (Model group) experienced an 11% body weight reduction compared to the CK group (Fig. 2B). In comparison, probiotics and VC treatments demonstrated protective effects against DSS-induced weight loss. Among them, the GR-3 group exhibited a higher protective effect against weight loss in the 11th week, 17% higher than the Model group (Fig. 2C). However, 5-FU group experienced a substantial weight drop during initial phase of DSS treatment (Fig. 2C). The survival rate of 5-FU group was also only 50%, significantly lower than that of the CK group (Fig. S4). In contrast, the survival rates of the GR-3 and GR-6 groups were 30% higher than that of the Model group. Similarly, the intervention with the probiotic *Pediococcus pentosaceus* increased the survival rate of AOM/DSS-treated mice by 30%[36]. After each dose of DSS administration, significant fluctuations in bleeding were observed (Fig. 2D). By day 68, the average occult blood score in Model group was 2 points, surpassing all intervention groups. Similarly, fecal consistency scores in the intervention groups consistently lower than the Model group (Fig. 2E).

Besides, the Model group exhibited significant colon shortening, averaging approximately 10 cm (Fig. 2F). However, treatment of probiotics, 5-FU, and VC prevented AOM/DSS-induced colon shortening (Fig. 2G). Notably, the colon length in the GR-3 group reached 12.03 cm. Compared to Model group, GR-3 and 5-FU treatments reduced tumor count by 51.2% and 52%, respectively (Fig. 2H). H&E staining was further performed to observe colonic structure (Fig. 2I up). The Model group samples presented with inflammatory cell infiltration, crypt epithelium irregularities, and mucosal degradation. In contrast, probiotics and VC treatments ameliorated colon dysplasia and structural abnormalities. Nonetheless, 5-FU did not mitigate inflammatory cell infiltration (Fig. 2I up). In addition, Alcian Blue staining showed that probiotics and VC treatments countered AOM/DSS induced goblet cell loss (Fig. 2I down). Similarly, 5-FU treatment failed to reverse this phenomenon.

L. fermentum GR-3 promotes apoptosis and inhibits tumor cell proliferation

The distal colon, known as the primary site for tumor occurrence[37], exhibited the presence of GR-3 in both its mucosa (Fig. 3A) and tumor tissues (Fig. 3B). In contrast, the abundance of GR-6 within the tumors was comparable to that observed in the Model group. This may facilitate GR-3 to directly exert its effects and promote apoptosis in tumor cells. As for proliferation and apoptosis related markers, apoptotic markers p53 and Bax were downregulated in distal colon tissue of Model group, while the GR-3,
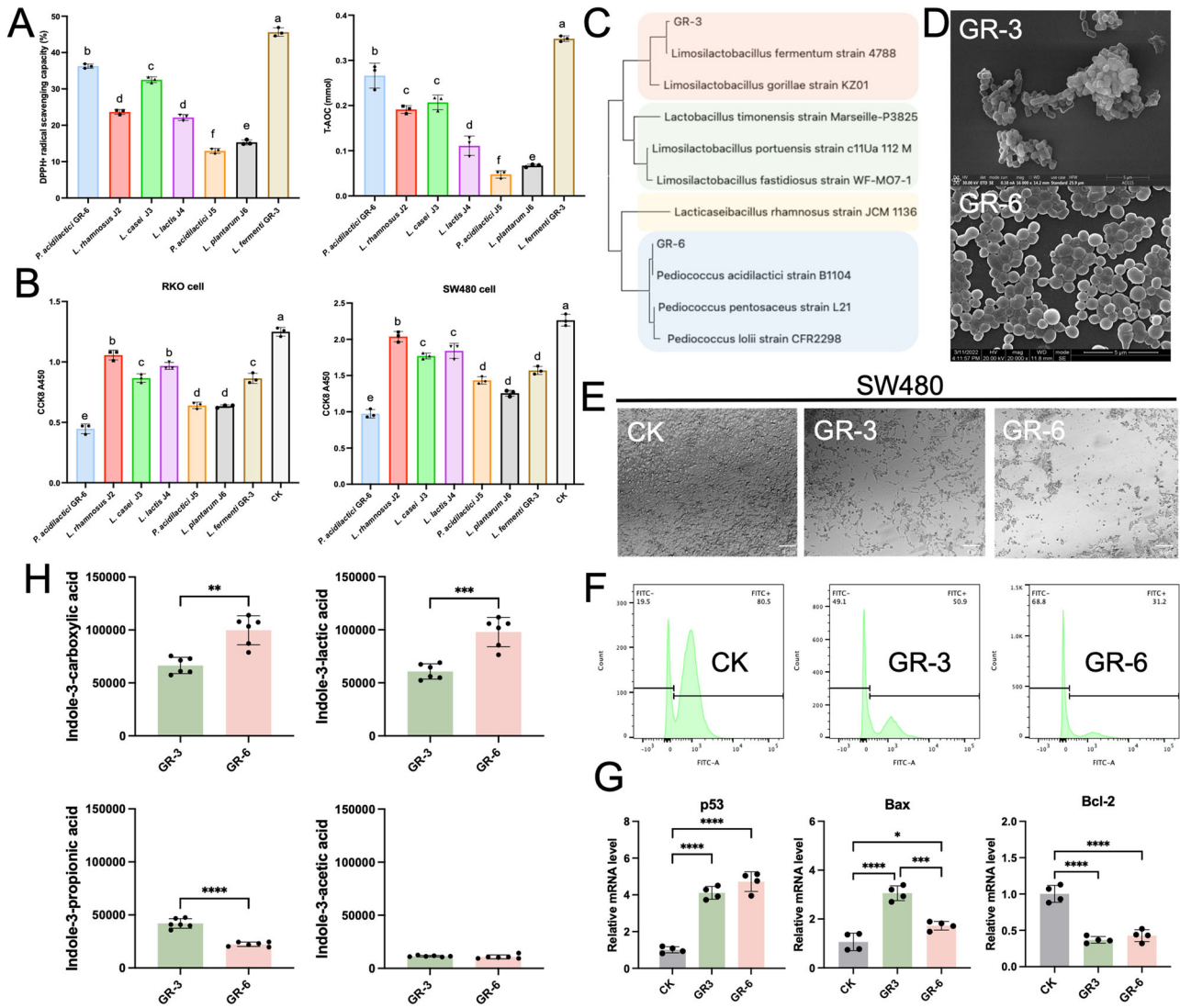
Fig. 1 | Characterization of strains GR-3 and GR-6 in vitro. A DPPH free radical scavenging capacity and total antioxidant capacity of different probiotics in vitro (mean ± SD; $n = 3$). T-AOC: total antioxidant capacity. **B** Cell viability of RKO and SW480 after incubation with different probiotics for 3 h (mean ± SD; $n = 3$). **C** Phylogenetic tree of strains GR-6, GR-3 and related bacteria. 16S rDNA sequences were aligned by ClustalW, and neighbor-Joining method was used to construct taxonomy tree. **D** Scanning electron microscope (SEM) morphology of strains GR-3 and GR-6. **E** Cell morphology of SW480 after incubation with strains GR-3 or GR-6 for 3 h (Bx53, Olympus; 40 × magnification). **F** The viability of SW480 cells was analyzed using flow cytometry following a 3-hour co-incubation with strains GR-3 or GR-6. Calcein-AM labeled cells exhibited green fluorescence and were classified into the FITC+ group, while the FITC- group represented the unlabeled cells. **G** mRNA expression levels of apoptotic markers p53, Bax and anti-apoptotic markers Bcl-2 in CT26 cells after co-incubation with GR-3 and GR-6 for 3 h (mean ± SD; $n = 4$). **H** Relative abundance of indole-3-carboxylic acid, indole-3-lactic acid, indole-3-propionic acid and indole-3-acetic acid in strains GR-3 or GR-6 (mean ± SD; $n = 6$). Different lowercase letters indicate significant differences between groups.

5-FU and VC treatments restored their mRNA levels (Fig. 3C, D). The mRNA levels of the anti-apoptotic marker Bcl-2 and tumor cell proliferation-related markers NF-κB and β-catenin were significantly increased in the Model group, but the GR-3 intervention reduced their abundances by 61%, 34%, and 55%, respectively (Fig. 3E–G). Some CXCR2 ligands, including Cxcl1, Cxcl2, and Cxcl5, which are related to the pathological progression of CRC[38], exhibited the upregulated expression in the Model group. However, this surge was mitigated with GR-3 treatment (Fig. 3H–J). qRT-PCR results were further confirmed by Immunohis-tochemistry (IHC) assays. Specifically, the positive expression rate of the apoptosis factor Bax was 18.98% in distal colon tissues of GR-3 group, which higher than in the Model group16.86% (Fig. 4K up). TLR4, a key regulator in CRC development[39], showed increased protein expression in Model group. Nevertheless, GR-3 treatment reduced its positive rate to 3.17% (Fig. 4K down). Moreover, the count of TUNEL-positive cells in GR-3 group was

1.96-fold higher than that in the Model group (Fig. 4L). These results mutually corroborate that GR-3 promoted apoptosis in distal colon tumor cells.

L. fermentum GR-3 mitigates oxidative stress, gut inflammation, and intestinal barrier damage induced by AOM/DSS

Gastrointestinal inflammation can cause intestinal mucosa damage, resulting in the presence of fecal occult blood[40]. Regarding the pro-inflammatory proteins in the colon and serum, the Model group exhibited a 10% ~ 80% increase in TNF-α, IL-1β, and IL-6 compared to the CK group (Fig. 4A–C). GR-3 intervention decreased the expression levels of these inflammatory cytokines, while GR-6 treatment still maintained high level of these cytokines. In contrast, 5-FU treatment enhanced IL-6 expression by 61% compare with Model group. When comparing different treatment groups, it was observed that the expression levels of TNF-α, IL-6, IL-1β and
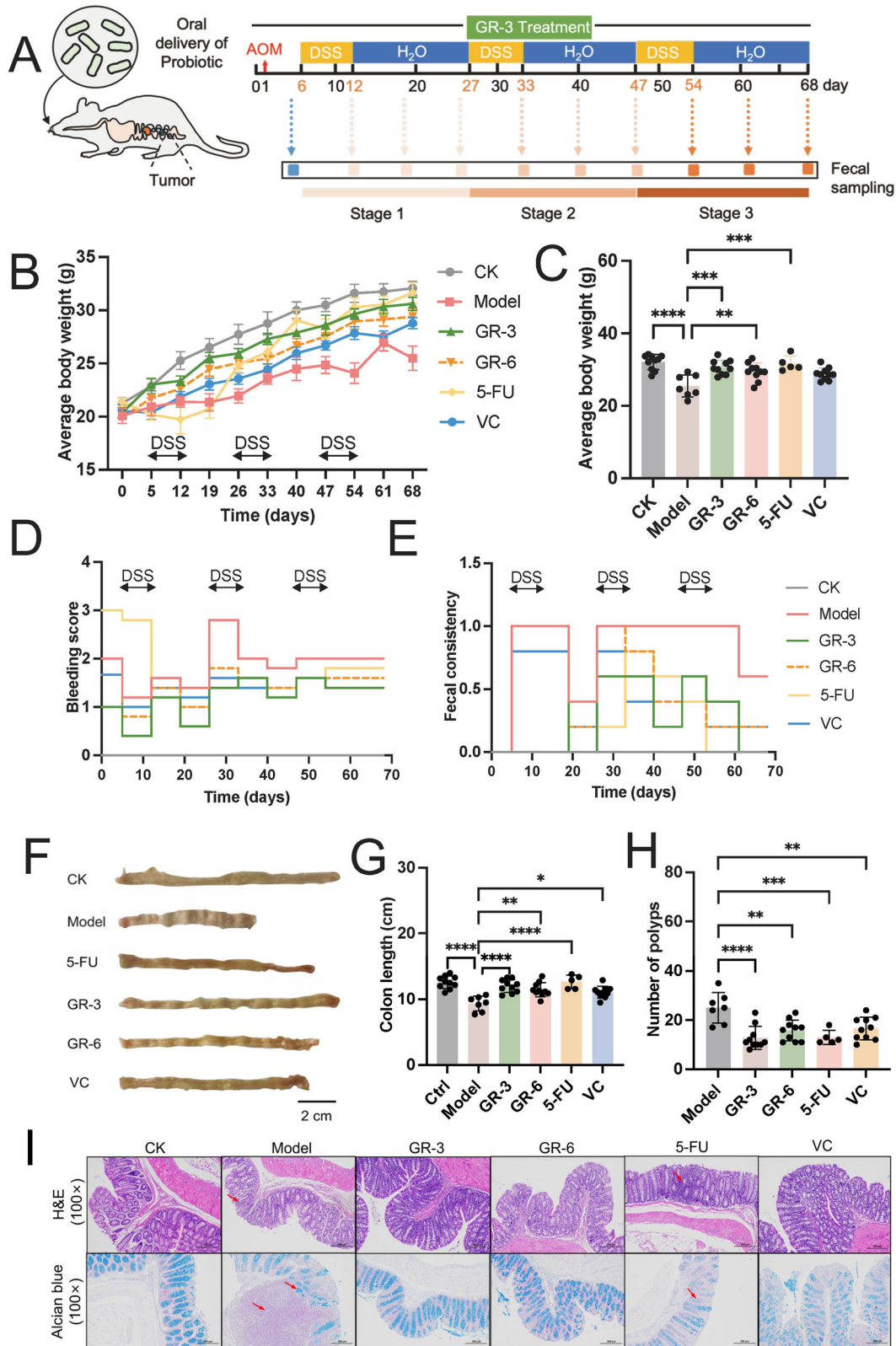
Fig. 2 | Effects of *L. fermentum* GR-3 on the tumor development in AOM/DSS-triggered CRC mouse model. A Experimental procedure for development of the AOM/DSS-induced CRC model and drugs administration. Mice received a single injection of AOM, followed by a week of 2% DSS water and two weeks of regular water, repeated thrice. *L. fermentum* GR-3, *P. acidilactici* GR-6 (both at 1×10^9 CFU), and vitamin C (VC, 100 mg/kg) were orally given to CRC mice. 5-FU (40 mg/kg) was injected intraperitoneally twice weekly. CK denotes the control group. **B** Variation in average mouse body weight across six groups (mean ± SEM). **C** Comparison of average body weight comparison on day 68 (mean ± SD; $n = 5$ for 5-FU group ; $n = 7$ for Model group; $n = 10$ for other groups). **D** Weekly bleeding scores determined by fecal occult blood tests range from 0 (normal, negative result) to 3 (strongly positive). **E** Weekly assessment of fecal consistency with 0 representing normal texture and 1 representing soft and sticky feces. **F** Image showcasing colon lengths of different groups. **G** Mean colon lengths across six groups (mean ± SD). **H** Incidence of colon tumors in each group (mean ± SD). **I** H&E and Alcian blue-stained representative colon sections from the groups (100 × magnification).
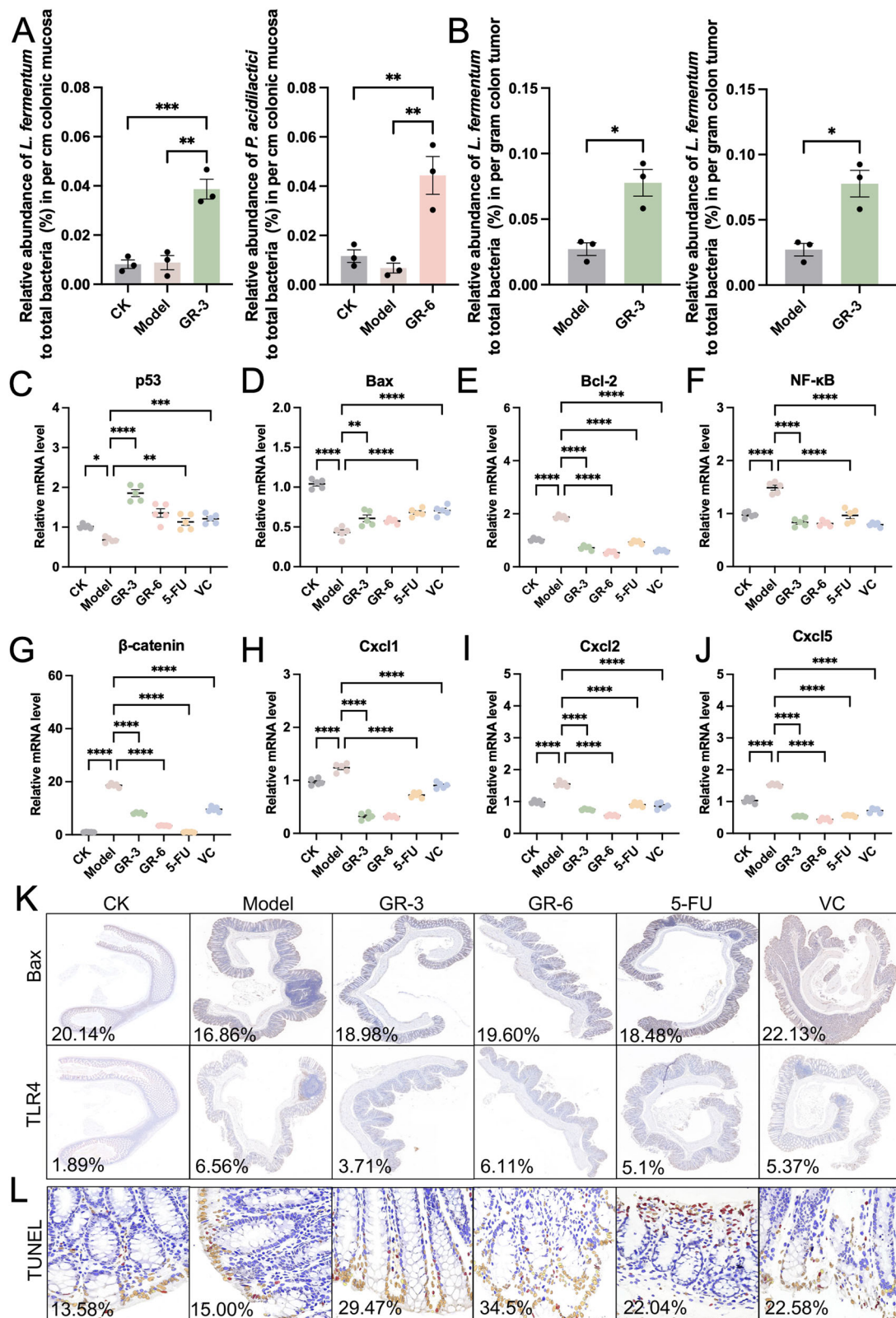
Fig. 3 | Effect of *L. fermentum* GR-3 on apoptosis-related immune response in the colon of mice. A Relative abundance of *L. fermentum* and *P. acidilactici* to total bacteria in per cm distal colonic mucosa (mean ± SD; $n = 3$). **B** Relative abundance of *L. fermentum* and *P. acidilactici* to total bacteria in per gram colon tumor (mean ± SD; $n = 3$). mRNA quantification of the pro-apoptosis markers p53 (**C**) and Bax (**D**), anti-apoptosis marker Bcl-2 (**E**), tumor cell proliferation markers NF-κB (**F**) andβ-catenin (**G**), CRC development related chemokines (Cxcl1, Cxcl2 and Cxcl3) (**H–J**) using qRT-PCR (mean ± SD; $n = 5$). The mRNA level was normalized with the mRNA level of GAPDH. **K** The expression levels of Bax and TLR4 in the mice colon were determined using immunohistochemistry. **L** Representative image of TUNEL staining on the mouse distal colon tissue. The positive rate of immunohistochemical images was analyzed using Aipathwell and marked in the lower left corner of the image.

Fig. 4 | Impact of *L. fermentum* GR-3 on oxidative stress, inflammatory response, and intestinal barrier in a CRC mouse model. A–C Protein levels of inflammatory cytokines TNF-α, IL-6 and IL-1β in colon and serum samples of mice in each group (mean ± SD; *n* = 4). mRNA quantification of anti-inflammatory cytokines IL-4 (**D**) and IL-10 (**E**), along with inflammatory related genes iNOS (**F**) and COX-2 (**G**) in colon tissues of mice in each group (mean ± SD; *n* = 5). The mRNA level was normalized with the mRNA level of GAPDH. **H**, **I** Serum and fecal total antioxidant capacity in each group (mean ± SD; *n* = 4). T-AOC: total antioxidant capacity. **J–L** The contents of oxidative stress marker MDA, antioxidants reduced GSH and SOD in colon and serum samples of mice in each group (mean ± SD; *n* = 5). **M** The content of mice serum LPS in each group (mean ± SD; *n* = 5). **N** The content of serum FITC-dextran in the intestinal barrier integrity analysis (mean ± SD; *n* = 3). (**O-R**) mRNA expression levels of mucin-associated proteins MUC2 (**O**) and TFF3 (**P**), along with tight-junction structural proteins ZO-1 (**Q**) and Occludin (**R**) (mean ± SD; *n* = 5). The mRNA level was normalized with the mRNA level of GAPDH.
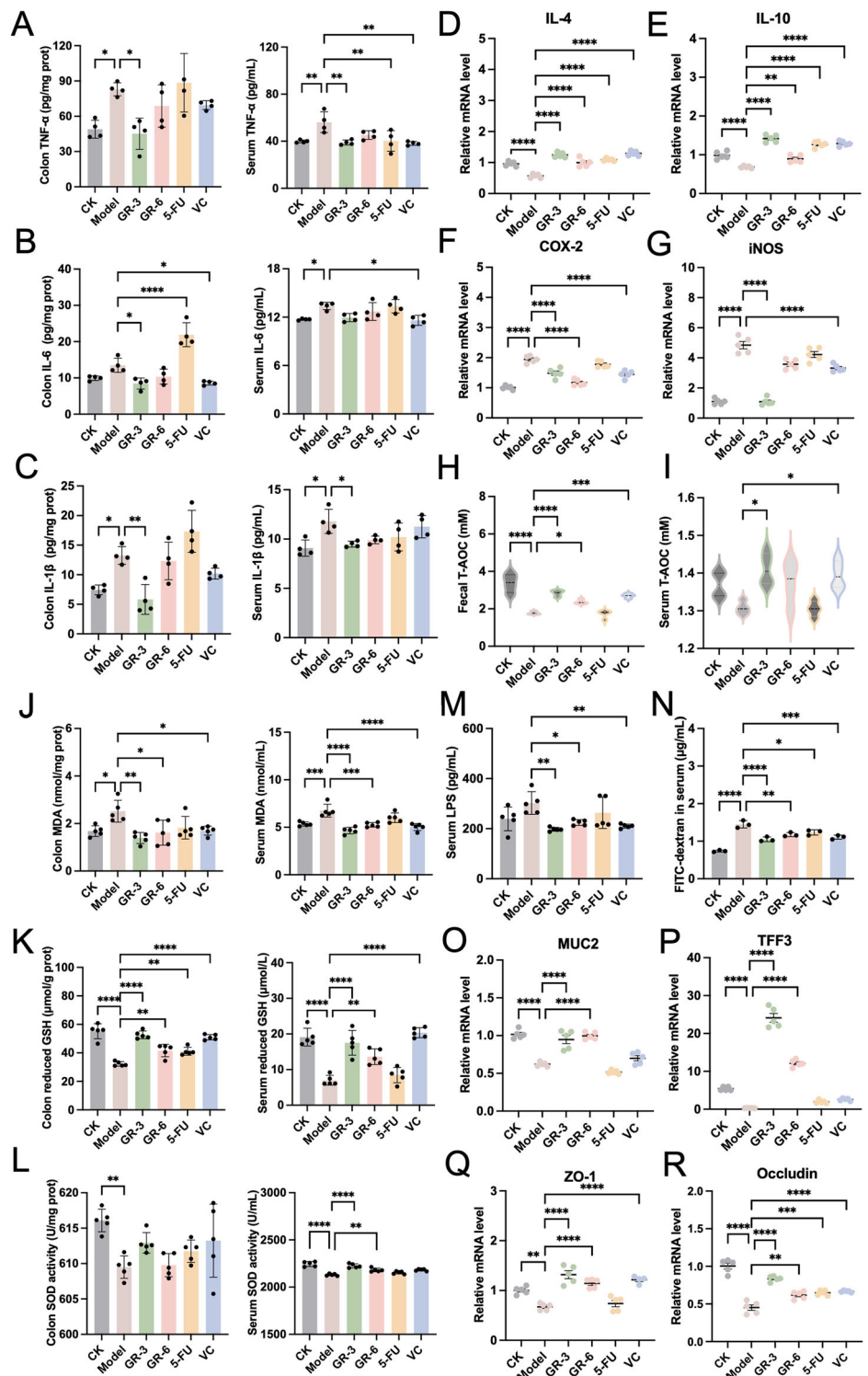
iNOS in the GR-3 group were lower than those in the 5-FU group (Table S4). Colon qRT-PCR analysis showed a similar trend (Fig. S4A–C). As for the anti-inflammatory cytokines IL-10 and IL-4, all therapeutic groups counteracted their diminished mRNA levels induced by AOM/DSS (Fig. 4D, E). The mRNA levels of inducible nitric oxide synthase (iNOS) and cyclooxygenase-2 (COX-2) were also examined. Compared to Model group, *iNOS* and *COX-2* were down-regulated by 81% and 22% after GR-3 treatment (Fig. 4F, G). However, neither GR-6 nor 5-FU treatment mitgated the abnormal expression of iNOS. Furthermore, the expression level of iNOS in the GR-3 group was also lower than that in the VC group (Table S4). During

inflammation, immune cells such as neutrophils and macrophages, produce reactive oxygen species[41]. The resulting oxidative stress can then activate NF-κB signaling pathways, further promoting inflammatory responses[42]. Consistent with the fecal DPPH· clearance test results (Fig. S6), both GR-3 and VC significantly improved total antioxidant capacity in fecal and serum samples, surpassing the levels observed in the 5-FU group (Fig. 4H–I, Table S4). The oxidation-reduction potential, which reflects the redox state of samples[43], was comparably reduced by GR-3 and VC interventions in the fecal samples of AOM/DSS mice (Fig. S7). Therefore, oxidative stress related markers were assessed in serum and colon tissues. Relative to Model group,

probiotics treatment reduced MDA levels (Fig. 4J) while restoring GSH and SOD levels (Fig. 4K, L). Serum analysis revealed that the SOD levels in the GR-3 group were significantly higher compared to the VC, GR-6, and 5-FU groups (Table S4). Additionally, 5-FU failed to reverse the AOM/DSS-induced disruption of serum MDA and GSH. To further evaluate the potential of probiotics in ameliorating intestinal barrier function, oral FITC-dextran was employed to assess intestinal permeability. AOM/DSS treatment increased serum FITC-dextran level, which was attenuated by strain GR-3 (Fig. 4M). Disruption of the intestinal barrier often results in elevated LPS levels[44]. Distinct from the negligible beneficial effects of 5-FU and VC treatment, probiotics intervention reversed the marked rise in serum LPS of Model group (Fig. 4N). Similarly, the expression of intestinal barrier integrity-associated proteins, including mucin-associated proteins such as mucin-2 (MUC2) and trefoil factor-3 (TFF3), as well as tight-junction structural proteins like zonula occludens-1 (ZO-1) and Occludin, were also reversed by administration of GR-3 (Fig. 4O–R). Conversely, the mRNA levels of MUC2, TFF3, ZO-1 and Occludin in the 5-FU group were lower than those in the GR-3 group (Table S4). These results suggest that *L. fermentum* GR-3 can alleviate the inflammatory response, oxidative stress and mitigate intestinal barrier damage induced by AOM/DSS.

L. fermentum GR-3 modulated gut microbiota composition

To determine the impact of AOM/DSS and therapeutic interventions on mouse gut microbiota, fecal samples underwent 16S rDNA analysis. Compared to the Model group, only VC group restored the Shannon and Chao1 index of intestinal microbiota compromised by AOM/DSS (Fig. 5A, B). PCoA anlyais based on Bray-Curtis dissimilarity revealed distinct separation between Model group and CK group (Fig. 5C). Apart from the GR-3 group, the intervention groups greatly shifted the gut microbiota of healthy mice (Fig. 5C). Relative to the CK group, the Model group exhibited a significant expansion of *Bacteroidaceae* and a decline in *Lachnospriraceae* (Fig. 5D). Analysis of the top 12 genera revealed that beneficial bacteria *Lactobacillus*[45], *Bifidobacterium*[46], *Alloprevotella*[47], and the short-chain fatty acids (SCFA) producer *Lachnospriraceae* _NK4A136_group[48] were reduced in the Model group, whereas inflammation-related bacterium *Bacteroides*[49] showed an expansion (Fig. 5E). In contrast, GR-3 intervention rescued the abundance of *Alloprevotella* and *Lachnospireaceae* _NK4A136_group and inhibited the expansion of *Bacteroides*. Compared to the GR-3 group, the GR-6 group exhibited higher abundances of *Alloprevotella* and *Bacteroides*, along with a lower abundance of *Lachnospiraceae*_NK4A136_group. Correlation cluster analysis at the genus level showcased that the gut microbiota of the CK group closely resembles that of the GR-3 group (Fig. 5E). Subsequent LEfSe analysis identified differential microorganisms between the CK & Model groups, and the Model & GR-3 groups (Fig. S8A, B). The finding indicated that GR3 reversed the expansion of *Dubosiella*, *Pseudoflavonifractor* and *Bacteroides* induced by AOM/DSS, and restored the abundance of HT002, *Alloprevotella*, *Lachnospiraceae*_NK4A136_group, *Rikenella* and *Bifidobacterium* diminished in Model group (Fig. S8C). Further correlation analysis revealed an antagonistic relationship between the cluster of *Dubosiella*, *Pseudoflavonifractor*, *Bacteroides* and the group comprising *Lachnospiraceae*_NK4A136_group, *Rikenella*, and *Bifidobacterium* (Fig. S8D). Besides, metagenomic analysis spotlighted that *Bacteroides* and *Lachnospiraceae* as the most distinct bacterial differences between the Model and GR-3 groups (Fig. 5F). Compared to the Model group, *Bacteroides fragilis* was reduced in the GR-3 group, while the abundance of butyrate-producing species *Muribaculum intestinale*[50] was increased. Next, the gene expression abundances of related vitamin biosynthesis, amino acid metabolism, sulfur metabolism were analyzed (Fig. 5G). Relative to the Model group, the GR-3 intervention upregulated *xseA*, *ALDH*, *bcd*, *ghrA*, *KamE*, *nasA*, *mmsA*, *cofD*, and down-regulated *hyuB*, *mtnK*, *pfkB*, *ulaD* in

gut microbiome (Fig. 5H). Therefore, GR-3 intervention can maintain the homeostasis of intestinal microbiota.

L. fermentum GR-3 altered intestinal microbial metabolites

To explore whether remission of AOM/DSS induced CRC is associated with gut microbial metabolism, the non-targeted metabolome profiles were analyzed based on intestinal digestive samples. PLS-DA distinctly separated the metabolite profiles of the Model and GR-3 groups (Fig. 6A). A comparison between the CK & Model, and Model & GR-3 groups identified 98 shared differential metabolites (Fig. S9). These metabolites were predominantly associated with the KEGG pathways of primary bile acid biosynthesis, bile secretion, and terpenoid-quinone biosynthesis (Fig. 6B). We further focused on the metabolism of vitamins, tryptophan, and bile acids. Differential metabolites enriched in vitamin digestion and absorption include Calciol (Vitamin D3), Calcitriol (1, 25-dihydroxy vitamin D3) and Chenodeoxycholate (Vitamin B12) (Fig. 6C). Although the Model group consumed Vitamin B12, Vitamin D3 and Calcitriol, the GR-3 intervention effectively replenished these metabolisms (Fig. 6D–F). Indole and its derivatives are integral to oxidative stress resistance[51]. The Model group displayed elevated tryptophan level, which was alleviated following GR-3 intervention (Fig. 6G). Furthermore, GR-3 treatment increased the abundance of IPA, ICA and its derivative indole-3-carboxylate (Figs. 6H and S10), which is consistent with the results of in vitro bacterial metabolome analysis (Fig. 1H). Secondary bile acids derived from gut microbes are closed associated with the colitis onset. GR-3 intervention significantly reduced the relative abundance of cholic acid (CA), lithocholic acid (LCA), and deoxycholic acid (DCA) compared with Model group (Fig. 6J–L). Given that bile acids facilitate the absorption of fat-soluble vitamins[52], spearman correlation analysis was performed for aforementioned metabolites (Fig. 6M). The results indicated that DCA was negatively correlated with Vitamin B12, Vitamin D3 and 1, 25-dihydroxy vitamin D3, while IPA was negatively correlated with DCA and L-tryptophan. SCFAs are pivotal in warding off intestinal ailments[53]. AOM/DSS treatment reduced the abundances of acetate, propionate, and butyrate in the intestinal contents of mice. On the contrary, the GR-3 intervention maintained the levels of these SCFAs, which was comparable to that of the CK group (Fig. S11). This result is consistent with the high abundance of SCFA producers in the gut microbiota. In summary, GR-3 intervention can ameliorate AOM/DSS induced intestinal microbial metabolic disorders.

Discussion

The gut microenvironment in CRC patients shows marked differences when compared to that of healthy individuals[54]. Recent research has emphasized the significance of the antioxidant properties of probiotics in CRC therapy[55]. Antioxidants such as N-acetylcysteine and NSAID, have demonstrated preventative effect against cancer[53,56]. In alignment with our findings, VC exhibited an inhibitory effect on AOM/DSS induced mouse CRC[57]. Notably, supplementation with GR-3 also enhanced antioxidant levels in stool and serum in mice. Jones et al. showed that *L. plantarum* can induce cytoprotection against oxidative damage through the Nrf2 pathway[58]. The Nrf2 signaling pathway has been associated with inflammatory CRC[59]. Therefore, it is necessary to explore whether strain GR-3 affect the Nrf2 pathway. While the in vitro cancer cell inhibitory effect was as not strong as the strain GR-6, *L. fermentum* GR-3 with notable antioxidant activity exhibited superior in vivo efficacy in CRC treatment. Compared to Model group, the GR-3 group exhibited a significant reduction in total tumor numbers and an increased colon length, suggesting a restorative effect of GR-3 on colon tissue. Similarly, *L. coryniformis* MXJ32 and *L. gasseri* 505, can ameliorate intestinal tumorigenesis in AOM/DSS-induced CRC mouse model[60,61]. The administration of strain GR-3 also increased the levels of pro-apoptotic factors p53 and Bax[62], but down-regulated the level of anti-apoptotic factor Bcl-2[63], suggesting the recovery of apoptosis. In

Fig. 5 | Impact of AOM/DSS and *L. fermentum* GR-3 on mouse gut microbiome. A Evaluation of microbial diversity using the Shannon index (mean ± SD; $n = 5$). **B** Assessment of microbial richness using the Chao1 index (mean ± SD; $n = 5$). **C** PCoA plot based on Bray-Curtis dissimilarity. The p value is derived from the PERMANOVA. **D** Circos plot illustrating the relationship of gut microbiota at the family level in each group. **E** Composition analysis of gut microbiota of mice in each group at genus level. Correlation cluster analysis is performed based on Bray-Curtis distance. **F** Heatmap representing the abundance of microbial species. **G** Relative abundance of KO genes involved in representative microbial metabolism. **H** Significant differential KO genes between Model group and GR-3 group (mean ± SD; $n = 3$).
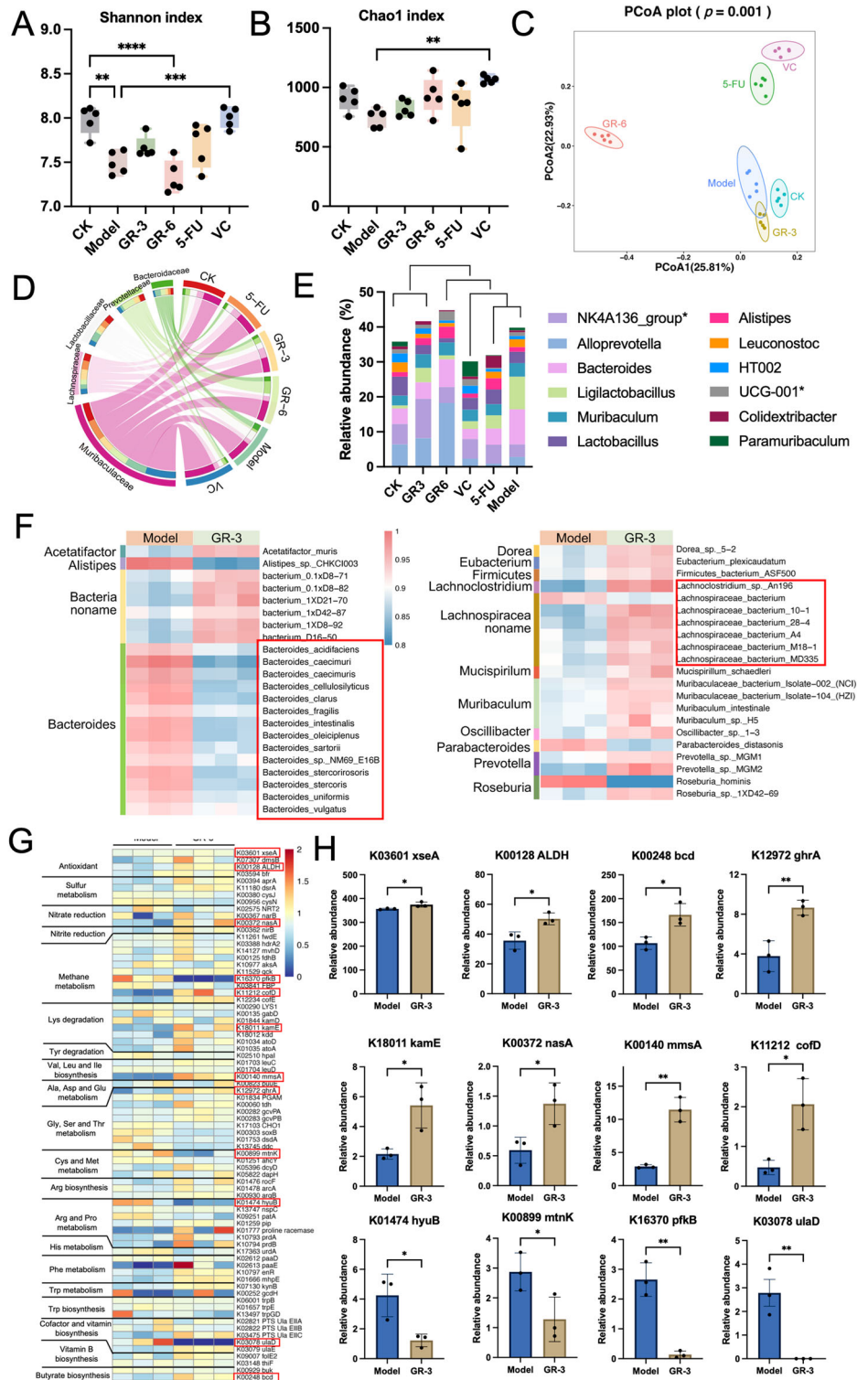
contrast, inhibition of apoptosis facilitates the survival of tumor cells in the Model group[64]. Histological analyses further corroborate the beneficial impacts of GR-3 on colon tissue, highlighting its protective effects against crypt damage, inflammatory infiltration, and goblet cell loss.

Chronic inflammation can lead to oxidative stress-induced DNA damage, which in turn activates oncogenes and deactivates tumor suppressor genes[65]. Supplementation of GR-3 effectively inhibited the increase of pro-inflammatory cytokines induced by AOM/DSS. The pro-inflammatory cytokine TNF-α can induce the expression of iNOS[66], and

the up-regulation of iNOS in the Model group may promote nitrogen oxide production, thereby affecting the progression of normal mucosa to metastatic cancer[67]. mRNA expression of CXCR2 ligands was also significantly decreased after GR-3 treatment. Irregular expression of these chemokines leads to the recruitment of inflammatory cells into the intestinal mucosa[68]. Similar down-regulation of these CXCR2 chemokines was observed in CRC mice treated with the Bifico probiotic cocktail and *Lactobacillus coryniformis* MXJ32[60,69]. Moreover, *L. fermentum* GR-3 administration suppressed the expression level of COX-2. COX-2 inhibitors have been shown to reduce
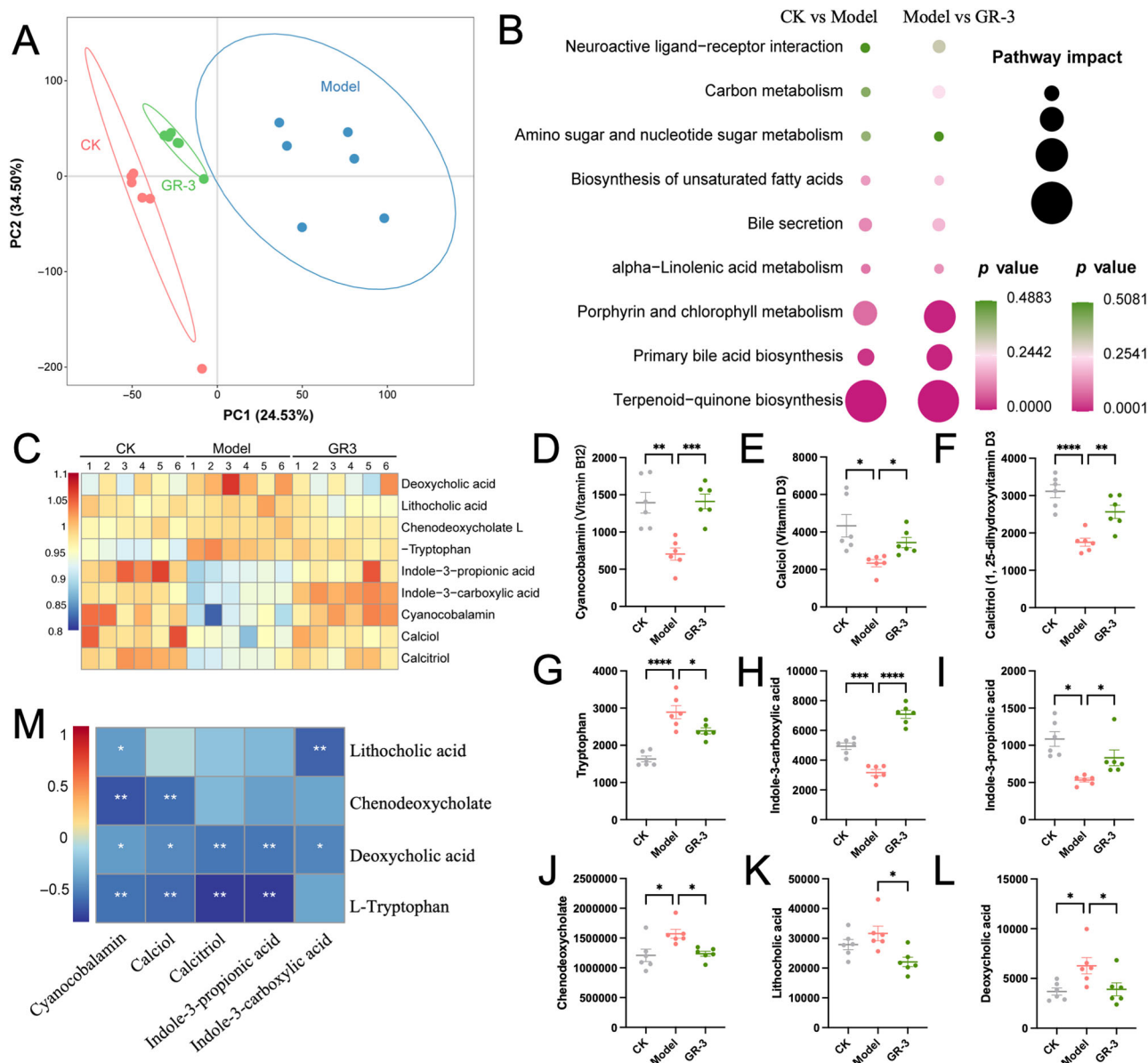
Fig. 6 | Impacts of AOM/DSS and *L. fermentum* GR-3 on gut microbiota metabolites. A PLS-DA visualization distinguishing intestinal metabolomes of CK, Model, and GR-3 groups. **B** Varied metabolic pathways between CK and Model groups, and between Model and GR-3 groups. **C** Heatmaps showcasing the distinct metabolites modified by AOM/DSS and GR-3 treatment relative to CK. Relative abundance comparison of Vitamin B12 (**D**), Vitamin D3 (**E**), Calcitriol (**F**), Tryptophan (**G**), Indole-3-carboxylate (**H**), Indole-3-propionic acid (**I**), Chenodeoxycholate (**J**), Lithocholic acid (**K**) and Deoxycholic acid (**L**) in fecal contents of each group (mean ± SD; n = 6). **M** Correlation matrix among various metabolites were obtained using a pairwise Spearman's rank correlation analysis. Correlations with adjusted *p* value less than 0.05 by the Benjamini-Hochberg FDR method are marked with white asterisk symbols.

CRC risk by reducing prostaglandin-mediated inflammation[70]. Chronic inflammation may also lead to damage to the intestinal mucosal layer and exacerbate bacterial translocation[71], as reflected in the increased serum LPS levels in the Model group. Meanwhile, LPS can trigger the TLR4 and NF-κB signaling pathway, inducing the expression of inflammatory factors and genes related to cancer cell proliferation[72,73]. In addition, the GR-3 intervention also restored the expression levels of intestinal barrier related genes. This indicates that GR-3 treatment prevents microorganisms from breaching the epithelial barrier into the circulatory system, thereby reducing the inflammatory response caused by gut pathogens. These evident suggested the antitumorigenic effect of strain GR-3 can be attributed to its anti-inflammation properties.

The presence of a microbial community within CRC tumors has been confirmed[74]. *Lactobacillus reuteri* can colonize tumors and inhibit tumor development by producing Reuterin[75]. Compared with strain GR-6, strain GR-3 can specifically colonize in tumor. This specificity ensures that the probiotic effectively targets the intended lesion site. Several probiotics are known to produce cancer-suppressing compounds that inhibit tumor progression. For example, *Lactobacillus plantarum* L168 and its metabolite indole-3-lactic acid ameliorated intestinal inflammation and gut microbiota dysregulation[76]. Indole-3-formaldehyde, released by *Lactobacillus tumorum*, can enhance the therapeutic effectiveness of immune checkpoint inhibitors[8]. Similarly, indole-3-lactic acid, derived from *Lactobacillus gallinarum*, has been proven to inhibit intestinal tumor formation in vivo[9]. In vitro experiments indicate that GR-3 can produce ICA and IPA. Consistent with it, an increased abundance of these metabolites was detected in the gut microbiota following GR-3 intervention. ICA inhibits the differentiation of CD4+ Treg cells and enhances the function of CD8 + T cells by regulating

Fig. 7 | The mechanism underlying the mitigation of AOM/DSS-induced CRC in mice by *L. fermentum* GR-3. AOM/DSS induces CRC by triggering intestinal inflammation, oxidative stress, gut microbiota dysbiosis, metabolic disruptions, and impaired intestinal barrier function. GR-3 exerts protective effects by modulating the gut microbiome and enhancing the production of beneficial metabolites such as SCFAs, indole derivatives, and vitamins. Additionally, GR-3 alleviates oxidative stress, diminishes inflammatory response, and restores intestinal barrier integrity.
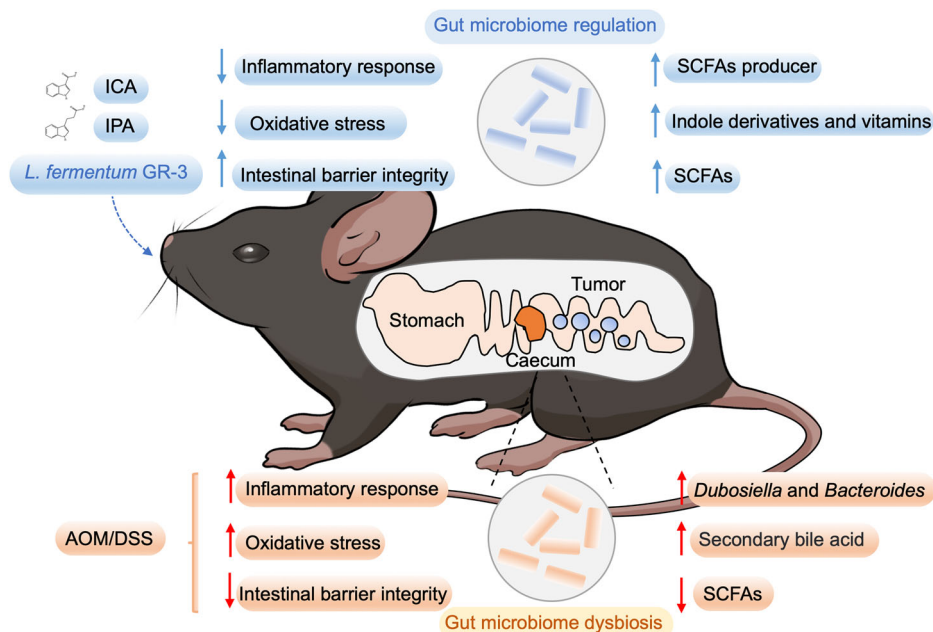
the IDO1/Kyn/AHR axis, thereby inhibiting the progression of CRC[77]. IPA, as a natural antioxidant, can effectively scavenge DPPH and ABTS free radicals and reduce DNA damage induced by oxidative stress[78,79]. Additionally, IPA can activate PXR, induce the expression of tight junction proteins, and antagonize TLR4/NFκB-mediated inflammatory response[80]. Jia et al., also demonstrated that IPA can activate precursor-exhausted T cells and enhance host anti-tumor immunity[81]. Therefore, GR-3 may activate the host's anti-tumor immune response, promote the intestinal barrier and antagonize the inflammatory response by regulating the abundances of intestinal metabolites ICA and IPA.

The above-mentioned study has confirmed the inhibitory effects of probiotics and their metabolites on CRC. However, research pertaining to the role of probiotics in modulating the gut microbiota has been limited. The heightened in vivo therapeutic efficacy of strain GR-3 relative to strain GR-6 establish a connection between its CRC therapy potential and gut microbiota remediation. The intestinal microbiota significantly affects the occurrence and formation of CRC[82]. GR-3 administration can restore AOM/DSS induced gut microbiota dysbiosis. The relative abundance of pro-inflammatory bacterium *Bacteroides* and *Dubosiella* was significantly increased in the Model group, accompanied by higher intestinal inflammation[83,84]. However, GR-3 treatment not only reversed the changes of these microbes, but also alleviated the inflammatory response. 16S rRNA sequencing indicates *Bacteroides* and *B. fragilis* were up regulated in the gut microbiota of CRC patients[85,86]. Enhanced colonization of *Bacteroides* is highly associated with the colon tumorigenesis[87]. *L. fermentum* GR-3 treatment also inhibited the expansion of *Pseudoflavonifractor*, which is considered a feature of CRC[88]. *Lactobacilli inhibits* the growth of CRC by inhibiting inflammation and angiogenesis[89]. In alignment with this study, metagenomic analysis had identified significant reductions in Lactobacillus in both early and late CRC[90]. Compared with the Model group, the GR-3 treatment maintained a higher abundance of *Alloprevotella*, *Lachnospiraceae*_NK4A136_group, *Rikenella*, *Bifidobacterium* and *Muribaculum intestinale*, all of which are recognized SCFAs producers[48,50,91,92]. Notably, a decline in butyrate-producing bacteria has been observed in CRC patients[93]. On the other hand, GR-3 intervention decreased the *ulaD* gene in the gut microbiota, potentially enhancing host VC uptake and reducing oxidative stress during VC degradation[94]. Furthermore, the upregulated *xseA* gene in the GR-3 group encodes superoxide dismutase, which eliminates superoxide radicals[95], while elevated *ALDH* genes alleviate oxidative stress by converting oxidative aldehydes into acids[96].

Supplementation with strain GR-3 also modulated metabolites in the gut microbiota, including Vitamin B12, Vitamin D3 and its active derivative calcitriol. Among them, Vitamin B12 participates in DNA synthesis and methylation, and it has been reported to reduce the risk of CRC[97,98]. Vitamin D is recognized for its anti-inflammatory properties and direct antineoplastic effects, including the inhibition of the NF-kB signaling pathway, interference with COX-2/PGE2 synthesis, and induction of tumor cell apoptosis and autophagic death[99,100]. GR-3 treatment also reduced the abundance of CA, DCA and LCA. CA stimulates invasion of human colon cancer cells[101], while LCA activates the TGR5 signal to inhibit the GSH production, causing the apoptosis and autophagy in dendritic cells[102]. Serum DCA level was correlated with the hyperplasia rate of colon mucosa[103]. Cong et al., demonstrated that DCA inhibits the response function of CD8 + T cells by targeting PMCA and suppressing NFAT2 signal transduction[104]. Interestingly, *Bacteroides* can transform CDCA and CA into LCA and DCA[105]. This suggests that *L. fermentum* GR-3 may reduce the risk of CRC by inhibiting the *Bacteroides* proliferation and regulating the bile acid metabolites. The increased abundance of SCFAs producers in the GR-3 group corresponds to higher levels of SCFAs. *Bcd* gene is involved in butyrate production, and its abundance is upregulated in the GR-3 group[106]. Correspondingly, the abundance of SCFAs producers and acetate, propionate, and butyrate in the gut microbiota of the GR-3 group increased. Acetate inhibited proliferation and induced apoptosis of CRC cells in a dose-dependent manner[107]. Butyrate exhibits anti-inflammatory properties in murine macrophage cells[108]. Recent reports indicate that SCFAs activate FFAR2 expressed in intestinal epithelial and immune cells, promoting the secretion of IL-10 and IL-22, regulating Treg differentiation, thereby preventing CRC and colonic inflammation[109]. Thus, the increase in SCFAs induced by GR-3 administration might also contribute to its anticancer efficacy.

Together, this study delves into the mechanisms underlying the preventive effects of GR-3 on CRC, specifically focusing on its antioxidant properties, immune regulation, intestinal barrier maintenance, and gut microecology modulation (Fig. 7). Contrary to conventional antioxidant therapy, *L. fermentum* GR-3 not only serves as an antioxidant, but also contributes to the regulation of intestinal homeostasis. Comparative analysis suggests that probiotics prevent CRC primarily through their regulation of the gut microbiota rather than their inherent potency. Additionally, the probiotic GR-3 is derived from traditional fermented foods, possesses high potential safety, and has been commercialized and marked. As an additive ingredient for "Jiangshui" yogurt, the safety of GR-3 far exceeds that

of many drugs[34]. More importantly, "Jiangshui" yogurt containing GR-3 has also demonstrated therapeutic effects on hyperuricemia in clinical trials[12]. Given the successful track record of *Lactobacillus reuteri* in anti-tumor research[110], we are optimistic that *L. fermentum* GR-3 will offer consumers with healthful options. Nevertheless, further analysis of the impact of strain GR-3 on specific immune responses and immune cell differentiation is needed. Additionally, it is essential to further elucidate the regulatory mechanisms of the gut microbiome and conduct human trials to ascertain the clinical efficacy of strain GR-3.

Methods and materials
Bacterial isolation, identification, and culture
Seven "Jiangshui" derived probiotics were isolated in Lanzhou, Gansu (36.06° N, 103.83° E), and stored in MRS broth (Solarbio Sci & Tech, Beijing, China) with 25% (v/v) glycerol at −20 °C. The strains were identified by aligning 16S rRNA gene sequencing, with sequences aligned to the NCBI database and submitted to GenBank (SUB11132737). Detailed information on the probiotic strains is provided in Table S1. Phylogenetic analysis was performed using MEGA 7.0 (Mega Co., Ltd., New Zealand), and their morphology was examined using scanning electron microscopy (Inspect, FEI, USA). The probiotics were incubated statically in the MRS broth (1:100 dilution) at 37 °C under aerobic condition for 16-24 h.

Cell lines and cell cultivation
RKO and SW480 human colon cancer cell lines were both purchased from Procell (Wuhan, China) and have been authenticated using STR profiling. All experiments were performed with mycoplasma-free cells. Cancer cells were cultured at 37 °C with 5% CO_2. The complete medium for these two cell lines was DMEM (Basal Medi, Shanghai, China), supplemented with 1% penicillin/streptomycin (P/S) (Gibco, USA) and 10% (v/v) fetal bovine serum (Gemini, USA).

In vitro co-culture of probiotics and CRC cells
Similar to earlier report[111], 2.5×10^4 colon cancer cells were seeded in 96-well cell culture plate containing 90 μL complete DMEM medium (without antibiotics). After 2 days incubation, colon cancer cells were cultured with 10 μL of probiotics culture ($OD_{600} = 0.6$) or MRS medium for 3 h at 37 °C. Bacteria were subsequently removed and replaced with fresh DMEM medium. The effect of bacterial cultures on RKO and SW480 cell viability was analyzed using CCK-8 kit (Beyotime, China). Cell morphology was observed using an inverted microscope (Carl Zeiss AG, Germany).

Determination of antioxidant capacity of probiotics in vitro
The probiotics were inoculated in 50 mL MRS broth at 37 °C overnight until the value of OD_{600} reached about 1. After centrifuging at 10, 000 g for 1 min, the medium was discarded, and the bacterial cells were resuspended with 10 mL cooled PBS (pH 7.4). The cell antioxidants were released by ultrasonic for 15 min, the resultant supernatants were obtained by following centrifuging at 12, 000 rpm, 4 °C for 5 min. Total antioxidant and DPPH free radical scavenging capacities were measured using commercial assay kits (Jiancheng Bioengineering Institute, China). The test data were calculated according to the formula of the manufacturer's instructions.

Flow cytometry analysis
Following incubation with the GR-3 or GR-6 strains for 3 h, the bacteria were washed away, and the CRC cells were then digested and resuspended in PBS (pH 7.4) at a quantity of 10^6 per sample. Subsequently, the SW480 cells were stained using the Calcein-AM Cell Viability Detection Kit (Beyotime, China). After a 30-minute incubation at 37°C in the dark, the cells were analyzed using flow cytometry (Dickinson and Company (BD), USA), with a total of 10,000 SW480 cells being counted. The cells emitting green fluorescence in the FITC channel were labeled as the FITC+ group, while those not labeled by Calcein-AM were categorized into the FITC- group. The flow cytometric data were processed and analyzed using FlowJo version 10.

Preparation of *L. fermentum* GR-3 and *P. acidilactici* GR-6 suspension
After harvesting the cultured *L. fermentum* GR-3 (deposited at CCTCC, no. M2021902) and *P. acidilactici* GR-6 by centrifuging at 5000 g for 10 min at 4 °C, the bacterial pellets were re-suspended in 10% autoclaved skimmed milk to a concentration of 5×10^9 CFU per mL, which were then divided into 2 mL portions and preserved at −80 °C for future use[11]. Each aliquot was thawed to room temperature prior to mouse oral gavage administration.

Animal experiment protocol
C57bL-6J female mice (6-week-old, about 22 ± 2 g average body weight) were purchased from Animal Center of Lanzhou University and housed in a specific pathogen-free facility with a constant temperature and humidity. Mice were randomly allocated into six groups, with 10 mice per group and 5 mice per cage. A partial double-blind method was adopted for the experiment. The mice grouping, treatment and data analysis were separated. During the 68 days, the animals were allowed free access to sterilized food and water. The control group (CK) was orally administrated with 200 μL PBS daily, while other treatments received AOM/DSS to induce CRC. As previously described[36], the mice were intraperitoneally injected with 10 mg kg^{-1} body weight AOM (MP Biomedicals, USA) on day 1. After 5 days, mice were orally given 2% (w/v) DSS (MW 36–50 kDa; A5486, Yeasen Biotech, China) for 1 week, followed by 2 weeks of regular drinking water, repeated thrice. The GR-3 and GR-6 groups were orally given with 200 μL (~1×10^9 CFU, six times a week) *L. fermentum* GR-3 and *P. acidilactii* GR-6 suspension, respectively. The 5-FU group received intraperitoneal injections of 5-Fluorouracil (5-FU) at a dose of 40 mg/kg body weight 5-FU (Beyotime, China) twice a week; whereas the VC group was orally administered 100 mg/kg body weight of fresh Vitamin C (sigma-Aldrich, USA) solution every day[57]. Mice's weight, fecal bleeding, and stool consistency were monitored weekly. The fecal bleeding analysis was measured using an occult blood reagent (Nanjing Jiancheng Bioengineering Institute, China) and scored as 0 = normal (negative test result), 1 = slight positive result, 2 = positive result, 3 = strong positive result. Fecal consistency was score as 0 = normal, 1 = soft and sticky. Fecal samples from mice in each group were collected on days[5,12,19,26,33,40,47,55,68], and then frozen at −80 °C. On day[68], mice were anesthetized with 1% sodium pentobarbital in normal saline (intraperitoneal injection, 40 mg/kg body weight). Blood samples were collected from mice posterior orbital plexus, centrifuged at $3000 \times g$ for 10 min, and the serum was obtained and stored at -80 °C. The mice were then euthanized by cervical dislocation. The entire colon was dissected longitudinally and rinsed with cold PBS (pH 7.4) to measure the colon length and number of polyps. After that, distal colon tissues (~1 cm) were removed, fixed with 4% paraformaldehyde (BL539A, Biosharp, China), and the remaining tissue was frozen at −80 °C until use.

Histopathological assays
The overnight fixed colon tissues were dehydrated with gradient ethanol, clarified with xylene, embedded in paraffin, then sliced into section of 5-μm thickness using a semi-auto microtome (RM2265, Leica, Germany). The prepared paraffin sections were stained with terminal deoxynucleotidyl transferase dUTP nick end labeling (TUNEL), alcian blue and hematoxylin and eosin (H&E). After antigen repair, the expression levels of B-cell lymphoma 2 (Bcl-2) associated X protein (Bax) and Toll-like receptor 4 (TLR4) in colon tissues were detected by immunohistochemistry. The specimens were observed and photographed using Olympus optical microscope (BX53, Tokyo, Japan) and the number of positive cells were analyzed using digital pathological image analysis software Aipathwell (Servicebio, China).

Biomarker analysis
Serum samples were thawed in ice from −80 °C. Frozen colon tissues were weighed and soaked in ice-cold sterile PBS in proportion (1: 9, w/v), then homogenized using automatic tissue dissociator (Tissuelyser-24L, Jingxin, Shanghai, China) and centrifuged at 5000 g for 5 min to collect supernatant. Then, serum lipopolysaccharides (LPS; FANKEWEI, China), colon

inflammatory cytokines (interleukin-6 (IL-6), interleukin-1 beta (IL-1β), tumor necrosis factor-alpha (TNF-α); Shanghai Enzyme-linked Biotechnology, China) and oxidative stress related biomarkers (malondialdehyde (MDA), glutathione (GSH) and superoxide dismutase (SOD); Nanjing Jiancheng Bioengineering Institute, China) were determined using corresponding ELISA kits. The total protein concentration in the homogenate supernatant was measured using a Bradford Protein Assay Kit (Beyotime, China, P0006).

Quantitation of gene expression in colon tissues
Total RNA from the colon tissue was extracted from individual homogenates with the RNAprep Pure Tissue Kit (DP431, TIANGEN Biotech) and reverse-transcribed into cDNA using the HiScript 1st Strand cDNA Synthesis kit (R111, Vazyme Biotech, China). Then, 100 ng of cDNA was mixed TB Green Premix Ex Taq II (RR802, Takara) and quantitative reverse transcription PCR (qRT-PCR) was performed on QuantStudio 5 (Applied Biosystems, Thermo Fisher Scientific, USA). The primer sequences of the target gene are listed in Table S3. GAPDH gene were used as internal controls, and the mRNA expression level of each gene was calculated using $2^{-\Delta\Delta Ct}$ method.

Intestinal barrier integrity analysis
Mice were fasted for 4 h before oral administration of fluorescein isothiocyanate (FITC)-dextran (3,000-5000 kDa, Sigma-Aldrich, 600 mg/kg body weight, 80 mg/mL PBS; pH 7.4), followed by further 4 h of fasting. Then, a total of 100 μL serum samples were mixed with an equal volume of PBS. The fluorescence intensity was immediately measured using a microplate reader (Varioskan Flash Thermo scientific) with an emission wavelength of 535 nm and excitation wavelength of 485 nm. The standard curve was established by diluting FITC-dextran in PBS.

Quantification of *L. fermentum* and *P. acidilactic* populations in mouse feces, distal colonic mucosa and tumor tissue
Following a 63-day experimental period, segments around 1 cm from the distal colon were promptly harvested and rinsed with a sterile 0.9% saline solution. These tissue sections were then longitudinally dissected, and the mucosa was gently scraped off to collect the mucosal samples. Total DNA of mouse colonic mucosa was extracted using Stool DNA Kit (Tiangen, China). For mouse colonic tumor samples, DNA were extracted using QIAamp DNA Mini Kit (Qiagen, Germany). Mouse fecal DNA was extracted using Stool DNA Kit (Tiangen, China) and stored in −80 °C. Specific primers for total bacteria[112], *L. fermentum*[112] and *P. acidilactici*[11] were employed to perform quantitative real-time PCR (qPCR) on QuantStudio 5 (Applied Biosystems, USA) (Table S2). A standard curve was generated using ten-fold serial dilutions of known concentrations of plasmid DNA containing the66 target sequences. The proportion of GR-3 and GR-6 in feces was estimated by the ratio of *L. fermentum* or *P. acidilactici* to total bacteria, calculated based on the standard curve[37].

Determination of antioxidant capacity of mice feces
Fresh mice stool samples were proportionally (1:5, w/v) resuspended with sterile PBS (pH = 7.0), mixed by vortex, and then treated with ultrasonication for 5 min to obtain cell-free extracts. After centrifugation at 8000 rpm for 2 min, 1 mL of supernatants were collected to determine total antioxidant capacity using commercial assay kits.

Analysis of short-chain fatty acid (SCFAs) in mouse feces
The concentration of SCFAs in feces were analyzed by gas chromatography-mass spectrometer (GC-MS)[11]. Briefly, 600 mg of stool was thawed and re-suspended with 1.2 mL PBS (pH 7.4), mixed by vortex, and centrifuged at 15, 000 g for 15 min at 4 °C. Then 200 μL supernatants were filtered by 0.22 μm filter and mixed with 50% (V/V) H_2SO_4 (100 μL) to acidify. After standing for 2 min, 0.4 mL diethyl ether was added and the extracted organic phase were detected by GC-MS workstation (ThermoFisher Scientific, Trace 1300, Singapore) equipped with FID detector and chromatographic

column (TG-WAxMS, 30 m × 0.25 mm, Thermo Scientific, USA). The SCFA levels in each sample were determined by referencing the standard solution.

Measurement of the oxidation-reduction potential of fecal samples
The oxidation-reduction potential (ORP) in fecal samples was measured using reported method, with slight modifications[113]. Briefly, fecal samples stored at −80 °C were weighed into 15 mL sterile centrifuge tubes. Subsequently, 0.2 g of feces was resuspended in 4 mL of sterile ultrapure water and vortexed until a homogeneous solution was obtained. Each group had three replicates. The homogenate was then transferred into a sterile 50 mL beaker, and a handheld ORP tester (KEDIDA, China) was used to record the reading at 1 minute. The ambient temperature was maintained at 25 °C to avoid temperature effects on ORP, and the tester featured automatic temperature compensation. The measurement electrode was platinum, and the reference electrode was silver/silver chloride. The equilibrium potential of the redox reaction was determined according to the Nernst Equation[114]:

$$E = E_0 + \frac{RT}{nF} \ln \frac{[\text{Ox}]}{[\text{Red}]}$$

E represents the electrode potential. E_0 denotes the standard electrode potential. R is the gas constant. T is the temperature. n is the number of moles of transferred electrons, and F is the Faraday constant. The concentrations of the oxidized and reduced species are denoted by [Ox] and [Red], respectively.

Fecal microbiota analysis based on 16S rRNA sequencing
After thawed in ice, DNA from 200 mg fecal samples was extracted using Stool DNA kit (D4015-01, OMEGA, USA). DNA quality was assessed via agarose gel electrophoresis and the Nanodrop 2000 (Thermo Scientific). The 16S rRNA gene was amplified using 27 F and 1492 R, and the sequencing was done on the Illumina NovaSeq 6000 (2 × 250 paired ends) at LianChuan Co., China. Analysis was performed with QIIME 2, including denoising with Cutadapt and DADA2, and amplicon sequence variants (ASV) tables generation and annotation using the SILVA database. Alpha-diversity was analyzed using Mothur v.1.31.0. Beta diversity was characterized using Principal Coordinate Analysis (PCoA) based on the Bray–Curtis distance, with Anosim analysis and Permutational Multivariate Analysis of Variance (PERMANOVA) assessing group dissimilarity. Linear discriminant analysis (LDA) effect size (LEfSe) ($P < 0.05$ and logarithmic LDA threshold score was set at 3.0) was used to determine discriminative genera between groups.

Metagenomic shotgun sequencing and analysis
Genomic DNA from fecal samples was fragmented to ~400 bp using Covaris ME220 (Covaris, USA) and libraries were prepared with the TruSeq nano DNA LT kit (Illumina, USA), followed sequencing on the NovaSeq 6000 platform (LianChuan Co., China). After adapter removal with cutadapt v1.9 and quality trimming with fqtrim v0.94, reads were filtered from host DNA using Bowtie v2.2.0. Read quality was assessed with FastQC, contigs were constructed, and coding regions predicted and clustered for unigenes. Gene sets were annotated against the NCBI Non-Redundant Protein Sequence and Kyoto Encyclopedia of Genes and Genomes (KEGG) databases using DIAMOND. Differential metagenomic species between groups were identified with Kruscal-Wallis test.

Bacterial and fecal untargeted metabolome analysis
For bacterial samples, strains GR-3 and GR-6 were cultured overnight in MRS medium, followed by centrifugation at 10,000 g for 10 min at 4 °C. A 0.2 g wet weight of bacterial precipitate was collected and frozen in liquid nitrogen for 4 h before being stored at

Article

−80 °C. Fecal samples were stored at −80 °C immediately after collection. The thawed sample was extracted using methanol/water (1:1, v/v) and the obtained material was dissolved in acetonitrile. The samples were analyzed using liquid phase gas chromatography (Thermo Scientific UltiMate 3000 HPLC) and mass spectrometry (TripleTOF6600) (LC-MS). The raw data were processed using Compound Discoverer 3.1.0 (Thermo Fisher Scientific, USA). Each ion was identified by combining m/z and retention (RT) data and metabolites were annotated based on Kyoto Encyclopedia of Genes and Genomes (KEGG) database. Partial least squares-discriminant analysis (PLS-DA) with 200 permutation tests was used to compare metabolome profiles between groups. Differences in metabolite concentrations between the two groups were assessed using two-tailed Student's t-tests.

Statistical analysis

Data were analyzed using GraphPad Prism 8.0 and presented as mean ± SD. Differences between multiple groups were assessed using one-way ANOVA with Tukey's post-hoc test or Kruskal-Wallis's test with Benjamini-Hochberg FDR correction. Survival curves for mice were plotted using Kaplan-Meier analysis and compared with the log-rank test. Statistically significant values are denoted by asterisks ($*p < 0.05$, $** p < 0.01$, $*** p < 0.001$).

Data availability

16S rRNA sequencing data deposited in Sequence Read Archive (SRA) of the National Center for Biotechnology Information (NCBI) with the accession number of SUB13310369. Metagenomic sequencing data of gut microbiome was also deposited in SRA database with accession number of SUB13799886. The raw LC-MS profiles for fecal metabolome analysis were deposited in Metabolights with accession number of MTBLS7843.

References

1. Patel, S. G., Karlitz, J. J., Yen, T., Lieu, C. H. & Boland, C. R. The rising tide of early-onset colorectal cancer: a comprehensive review of epidemiology, clinical features, biology, risk factors, prevention, and early detection. *Lancet Gastroenterol. Hepatol.* **7**, 262–274 (2022).
2. Johnson, I. & Lund, E. Nutrition, obesity and colorectal cancer. *Alimentary Pharmacol. therapeutics* **26**, 161–181 (2007).
3. Johdi, N. A. & Sukor, N. F. Colorectal Cancer Immunotherapy: Options and Strategies. *Front Immunol.* **11**, 1624 (2020).
4. Weitz, J. et al. Colorectal cancer. *Lancet* **365**, 153–165 (2005).
5. Marijnen, C. A. et al. Impact of short-term preoperative radiotherapy on health-related quality of life and sexual functioning in primary rectal cancer: report of a multicenter randomized trial. *J. Clin. Oncol.* **23**, 1847–1858 (2005).
6. Kim, J. H. Chemotherapy for colorectal cancer in the elderly. *World J. Gastroenterol.* **21**, 5158–5166 (2015).
7. Longley, D. B., Harkin, D. P. & Johnston, P. G. 5-fluorouracil: mechanisms of action and clinical strategies. *Nat. Rev. Cancer* **3**, 330–338 (2003).
8. Bender, M. J. et al. Dietary tryptophan metabolite released by intratumoral Lactobacillus reuteri facilitates immune checkpoint inhibitor treatment. *Cell* **186**, 1846–1862.e1826 (2023).
9. Sugimura, N. et al. Lactobacillus gallinarum modulates the gut microbiota and produces anti-cancer metabolites to protect against colorectal tumourigenesis. *Gut* **71**, 2011–2021 (2021).
10. Li, Q. et al. Streptococcus thermophilus Inhibits Colorectal Tumorigenesis Through Secreting β-Galactosidase. *Gastroenterology* **160**, 1179–1193.e1114 (2021).
11. Feng, P. et al. Tibet plateau probiotic mitigates chromate toxicity in mice by alleviating oxidative stress in gut microbiota. *Commun. Biol.* **3**, 242 (2020).
12. Zhao, S. et al. Probiotic Limosilactobacillus fermentum GR-3 ameliorates human hyperuricemia via degrading and promoting excretion of uric acid. *iScience* **25**, 105198 (2022).
13. Feng, P. et al. Human supplementation with Pediococcus acidilactici GR-1 decreases heavy metals levels through modifying the gut microbiota and metabolome. *NPJ Biofilms Microbiomes* **8**, 63 (2022).
14. Ji, J., Jin, W., Liu, S. J., Jiao, Z. & Li, X. Probiotics, prebiotics, and postbiotics in health and disease. *MedComm* **4**, e420 (2023).
15. Zheng, D. W. et al. Prebiotics-Encapsulated Probiotic Spores Regulate Gut Microbiota and Suppress Colon Cancer. *Adv. Mater.* **32**, e2004529 (2020).
16. Yu, H. et al. Fecal microbiota transplantation inhibits colorectal cancer progression: Reversing intestinal microbial dysbiosis to enhance anti-cancer immune responses. *Front Microbiol* **14**, 1126808 (2023).
17. Serafini, M. & Del Rio, D. Understanding the association between dietary antioxidants, redox status and disease: is the total antioxidant capacity the right tool? *Redox Rep.* **9**, 145–152 (2004).
18. Sies, H. & Ursini, F. Homeostatic control of redox status and health. *IUBMB life* **74**, 24–28 (2022).
19. Rahman, T., Hosen, I., Islam, M. T. & Shekhar, H. U. Oxidative stress and human health. (2012).
20. Sies, H. Oxidative stress: oxidants and antioxidants. *Exp. Physiol.: Translation Integr.* **82**, 291–295 (1997).
21. Sen, S. & Chakraborty, R. in *Oxidative stress: diagnostics, prevention, and therapy* 1-37 (ACS Publications, 2011).
22. Aruoma, O. I. Free radicals, oxidative stress, and antioxidants in human health and disease. *J. Am. Oil Chem.' Soc.* **75**, 199–212 (1998).
23. Kondo, K., Sano, R., Goto, K., Hiramoto, K. & Ooi, K. Administration of High-Dose Vitamin C and Irinotecan Ameliorates Colorectal Cancer Induced by Azoxymethane and Dextran Sodium Sulfate in Mice. *Biol. Pharm. Bull.* **41**, 1797–1803 (2018).
24. Zhang, W. et al. Gut Microbiota-Derived Metabolites in Colorectal Cancer: The Bad and the Challenges. *Front Oncol.* **11**, 739648 (2021).
25. Weng, M.-T. et al. Microbiota and gastrointestinal cancer. *J. Formos. Med. Assoc.* **118**, S32–S41 (2019).
26. Arthur, J. C. et al. Intestinal inflammation targets cancer-inducing activity of the microbiota. *Science* **338**, 120–123 (2012).
27. Payne, C. M., Bernstein, C., Dvorak, K. & Bernstein, H. Hydrophobic bile acids, genomic instability, Darwinian selection, and colon carcinogenesis. *Clin. Exp. Gastroenterol.* **1**, 19–47 (2008).
28. Aboelella, N. S., Brandle, C., Kim, T., Ding, Z. C. & Zhou, G. Oxidative Stress in the Tumor Microenvironment and Its Relevance to Cancer Immunotherapy. *Cancers (Basel)* **13** https://doi.org/10.3390/cancers13050986 (2021).
29. Eslami, M. et al. Importance of probiotics in the prevention and treatment of colorectal cancer. *J. Cell Physiol.* **234**, 17127–17143 (2019).
30. Chen, P. et al. Cultivation-independent comprehensive investigations on bacterial communities in serofluid dish, a traditional Chinese fermented food. *Genom. Data* **7**, 127–128 (2016).
31. Yang, T. et al. High Antioxidant Capacity of Lacticaseibacillus paracasei TDM-2 and Pediococcus pentosaceus TCM-3 from Qinghai Tibetan Plateau and Their Function towards Gut Modulation. *Foods* **12** https://doi.org/10.3390/foods12091814 (2023).
32. Wu, Y. et al. Limosilactobacillus fermentum JL-3 isolated from "Jiangshui" ameliorates hyperuricemia by degrading uric acid. *Gut Microbes* **13**, 1–18 (2021).

33. Cheng, Y., Ling, Z. & Li, L. The Intestinal Microbiota and Colorectal Cancer. *Front Immunol.* **11**, 615056 (2020).

34. Bell, H. N. et al. Reuterin in the healthy gut microbiome suppresses colorectal cancer growth through altering redox balance. *Cancer Cell* **40**, 185–200.e186 (2022).

35. dos Reis, S. A. et al. Review of the mechanisms of probiotic actions in the prevention of colorectal cancer. *Nutr. Res.* **37**, 1–19 (2017).

36. Chung, Y. et al. A synthetic probiotic engineered for colorectal cancer therapy modulates gut microbiota. *Microbiome* **9**, 122 (2021).

37. Tang, H. et al. Tumor-targeting engineered probiotic Escherichia coli Nissle 1917 inhibits colorectal tumorigenesis and modulates gut microbiota homeostasis in mice. *Life Sci.* **324**, 121709 (2023).

38. Katoh, H. et al. CXCR2-expressing myeloid-derived suppressor cells are essential to promote colitis-associated tumorigenesis. *Cancer Cell* **24**, 631–644 (2013).

39. Burgueño, J. F. et al. Epithelial TLR4 Signaling Activates DUOX2 to Induce Microbiota-Driven Tumorigenesis. *Gastroenterology* **160**, 797–808.e796 (2021).

40. Foell, D., Wittkowski, H. & Roth, J. Monitoring disease activity by stool analyses: from occult blood to molecular markers of intestinal inflammation and damage. *Gut* **58**, 859–868 (2009).

41. Nagata, M. Inflammatory cells and oxygen radicals. *Curr. Drug Targets Inflamm. Allergy* **4**, 503–504 (2005).

42. Reuter, S., Gupta, S. C., Chaturvedi, M. M. & Aggarwal, B. B. Oxidative stress, inflammation, and cancer: how are they linked? *Free Radic. Biol. Med.* **49**, 1603–1616 (2010).

43. Agarwal, A. et al. A multicenter study to evaluate oxidative stress by oxidation–reduction potential, a reliable and reproducible method. *Andrology* **5**, 939–945 (2017).

44. Mohammad, S. & Thiemermann, C. Role of Metabolic Endotoxemia in Systemic Inflammation and Potential Interventions. *Front Immunol.* **11**, 594150 (2020).

45. Huang, R. et al. Lactobacillus and intestinal diseases: Mechanisms of action and clinical applications. *Microbiol Res.* **260**, 127019 (2022).

46. Mills, S., Yang, B., Smith, G. J., Stanton, C. & Ross, R. P. Efficacy of Bifidobacterium longum alone or in multi-strain probiotic formulations during early life and beyond. *Gut Microbes* **15**, 2186098 (2023).

47. Kong, C., Gao, R., Yan, X., Huang, L. & Qin, H. Probiotics improve gut microbiota dysbiosis in obese mice fed a high-fat or high-sucrose diet. *Nutrition* **60**, 175–184 (2019).

48. Ma, L. et al. Spermidine improves gut barrier integrity and gut microbiota function in diet-induced obese mice. *Gut Microbes* **12**, 1–19 (2020).

49. Parker, B. J., Wearsch, P. A., Veloo, A. C. M. & Rodriguez-Palacios, A. The Genus Alistipes: Gut Bacteria With Emerging Implications to Inflammation, Cancer, and Mental Health. *Front. Immunol.* **11**, 906 (2020).

50. Medina-Larqué, A. S. et al. Cranberry polyphenols and agave agavins impact gut immune response and microbiota composition while improving gut barrier function, inflammation, and glucose metabolism in mice fed an obesogenic diet. *Front Immunol.* **13**, 871080 (2022).

51. Ala, M. Tryptophan metabolites modulate inflammatory bowel disease and colorectal cancer by affecting immune system. *Int Rev. Immunol.* **41**, 326–345 (2022).

52. Bertolini, A., Fiorotto, R. & Strazzabosco, M. Bile acids and their receptors: modulators and therapeutic targets in liver inflammation. *Semin Immunopathol.* **44**, 547–564 (2022).

53. Gao, P. et al. HIF-dependent antitumorigenic effect of antioxidants in vivo. *Cancer Cell* **12**, 230–238 (2007).

54. Ahmad Kendong, S. M., Raja Ali, R. A., Nawawi, K. N. M., Ahmad, H. F. & Mokhtar, N. M. Gut Dysbiosis and Intestinal Barrier Dysfunction: Potential Explanation for Early-Onset Colorectal Cancer. *Front Cell Infect. Microbiol* **11**, 744606 (2021).

55. Molska, M. & Reguła, J. Potential Mechanisms of Probiotics Action in the Prevention and Treatment of Colorectal Cancer. *Nutrients* **11** https://doi.org/10.3390/nu11102453 (2019).

56. Michalowski, J. COX-2 inhibitors: cancer trials test new uses for pain drug. *J. Natl Cancer Inst.* **94**, 248–249 (2002).

57. Jeon, H. J. et al. Effect of vitamin C on azoxymethane (AOM)/dextran sulfate sodium (DSS)-induced colitis-associated early colon cancer in mice. *Nutr. Res. Pr.* **12**, 101–109 (2018).

58. Jones, R. M. et al. Lactobacilli Modulate Epithelial Cytoprotection through the Nrf2 Pathway. *Cell Rep.* **12**, 1217–1225 (2015).

59. Niture, S. K., Khatri, R. & Jaiswal, A. K. Regulation of Nrf2-an update. *Free Radic. Biol. Med.* **66**, 36–44 (2014).

60. Wang, T. et al. Lactobacillus coryniformis MXJ32 administration ameliorates azoxymethane/dextran sulfate sodium-induced colitis-associated colorectal cancer via reshaping intestinal microenvironment and alleviating inflammatory response. *Eur. J. Nutr.* **61**, 85–99 (2022).

61. Oh, N. S., Lee, J. Y., Kim, Y. T., Kim, S. H. & Lee, J. H. Cancer-protective effect of a synbiotic combination between Lactobacillus gasseri 505 and a Cudrania tricuspidata leaf extract on colitis-associated colorectal cancer. *Gut Microbes* **12**, 1785803 (2020).

62. Green, D. R. & Llambi, F. Cell Death Signaling. *Cold Spring Harb Perspect Biol* **7** https://doi.org/10.1101/cshperspect.a006080 (2015).

63. Jin, L. et al. YAP inhibits autophagy and promotes progression of colorectal cancer via upregulating Bcl-2 expression. *Cell Death Dis.* **12**, 457 (2021).

64. Pfeffer, C. M. & Singh, A. T. K. Apoptosis: A Target for Anticancer Therapy. *Int J Mol Sci* **19** https://doi.org/10.3390/ijms19020448 (2018).

65. Shah, S. C. & Itzkowitz, S. H. Colorectal Cancer in Inflammatory Bowel Disease: Mechanisms and Management. *Gastroenterology* **162**, 715–730.e713 (2022).

66. Suschek, C. V., Schnorr, O. & Kolb-Bachofen, V. The role of iNOS in chronic inflammatory processes in vivo: is it damage-promoting, protective, or active at all? *Curr. Mol. Med.* **4**, 763–775 (2004).

67. Payne, C. M., Bernstein, C., Bernstein, H., Gerner, E. W. & Garewal, H. Reactive nitrogen species in colon carcinogenesis. *Antioxid. Redox Signal* **1**, 449–467 (1999).

68. Wang, D., Dubois, R. N. & Richmond, A. The role of chemokines in intestinal inflammation and cancer. *Curr. Opin. Pharm.* **9**, 688–696 (2009).

69. Song, H. et al. Pretreatment with probiotic Bifico ameliorates colitis-associated cancer in mice: Transcriptome and gut flora profiling. *Cancer Sci.* **109**, 666–677 (2018).

70. Rao, C. V. & Reddy, B. S. NSAIDs and chemoprevention. *Curr. Cancer Drug Targets* **4**, 29–42 (2004).

71. Yao, D., Dong, M., Dai, C. & Wu, S. Inflammation and Inflammatory Cytokine Contribute to the Initiation and Development of Ulcerative Colitis and Its Associated Cancer. *Inflamm. Bowel Dis.* **25**, 1595–1602 (2019).

72. Peng, C., Ouyang, Y., Lu, N. & Li, N. The NF-κB Signaling Pathway, the Microbiota, and Gastrointestinal Tumorigenesis: Recent Advances. *Front Immunol.* **11**, 1387 (2020).

73. Lu, Y. C., Yeh, W. C. & Ohashi, P. S. LPS/TLR4 signal transduction pathway. *Cytokine* **42**, 145–151 (2008).

74. Liu, W. et al. Microbial Community Heterogeneity Within Colorectal Neoplasia and its Correlation With Colorectal Carcinogenesis. *Gastroenterology* **160**, 2395–2408 (2021).

75. Mu, Q., Tavella, V. J. & Luo, X. M. Role of Lactobacillus reuteri in Human Health and Diseases. *Front Microbiol* **9**, 757 (2018).

76. Han, J. X. et al. Microbiota-derived tryptophan catabolites mediate the chemopreventive effects of statins on colorectal cancer. *Nat. Microbiol* **8**, 919–933 (2023).

77. Fong, W. et al. Lactobacillus gallinarum-derived metabolites boost anti-PD1 efficacy in colorectal cancer by inhibiting regulatory T cells through modulating IDO1/Kyn/AHR axis. *Gut* https://doi.org/10.1136/gutjnl-2023-329543 (2023).

78. Karbownik, M. et al. Indole-3-propionic acid, a melatonin-related molecule, protects hepatic microsomal membranes from iron-induced oxidative damage: relevance to cancer reduction. *J. Cell. Biochem.* **81**, 507–513 (2001).

79. Xu, C. et al. Antioxidant, antibacterial, and antibiofilm properties of polyphenols from muscadine grape (Vitis rotundifolia Michx.) pomace against selected foodborne pathogens. *J. Agric. food Chem.* **62**, 6640–6649 (2014).

80. Wlodarska, M. et al. Indoleacrylic acid produced by commensal peptostreptococcus species suppresses inflammation. *Cell host microbe* **22**, 25–37.e26 (2017).

81. Jia, D. et al. Microbial metabolite enhances immunotherapy efficacy by modulating T cell stemness in pan-cancer. *Cell.* **187**, 1651–1665.e21 (2024).

82. Wong, S. H. & Yu, J. Gut microbiota in colorectal cancer: mechanisms of action and clinical applications. *Nat. Rev. Gastroenterol. Hepatol.* **16**, 690–704 (2019).

83. Wick, E. C. et al. Stat3 activation in murine colitis induced by enterotoxigenic Bacteroides fragilis. *Inflamm. Bowel Dis.* **20**, 821–834 (2014).

84. Shang, J. et al. Exploring the mechanism of action of Sanzi formula in intervening colorectal adenoma by targeting intestinal flora and intestinal metabolism. *Front Microbiol* **13**, 1001372 (2022).

85. Sobhani, I. et al. Microbial dysbiosis in colorectal cancer (CRC) patients. *PLoS One* **6**, e16393 (2011).

86. Chen, W., Liu, F., Ling, Z., Tong, X. & Xiang, C. Human intestinal lumen and mucosa-associated microbiota in patients with colorectal cancer. *PLoS One* **7**, e39743 (2012).

87. Baxter, N. T., Zackular, J. P., Chen, G. Y. & Schloss, P. D. Structure of the gut microbiome following colonization with human feces determines colonic tumor burden. *Microbiome* **2**, 20 (2014).

88. Ai, D. et al. Identifying Gut Microbiota Associated With Colorectal Cancer Using a Zero-Inflated Lognormal Model. *Front Microbiol*. **10**, 826 (2019).

89. Chattopadhyay, I. et al. Exploring the Role of Gut Microbiome in Colon Cancer. *Appl. Biochem. Biotechnol.* **193**, 1780–1799 (2021).

90. Yachida, S. et al. Metagenomic and metabolomic analyses reveal distinct stage-specific phenotypes of the gut microbiota in colorectal cancer. *Nat. Med*. **25**, 968–976 (2019).

91. Wang, X. et al. Fenofibrate Ameliorated Systemic and Retinal Inflammation and Modulated Gut Microbiota in High-Fat Diet-Induced Mice. *Front Cell Infect. Microbiol*. **12**, 839592 (2022).

92. Shi, H. et al. Dietary fucoidan of Acaudina molpadioides alters gut microbiota and mitigates intestinal mucosal injury induced by cyclophosphamide. *Food Funct.* **8**, 3383–3393 (2017).

93. Wang, T. et al. Structural segregation of gut microbiota between colorectal cancer patients and healthy volunteers. *Isme j.* **6**, 320–329 (2012).

94. Campos, E. et al. Aerobic L-ascorbate metabolism and associated oxidative stress in Escherichia coli. *Microbiology* **153**, 3399–3408 (2007).

95. Johnson, F. & Giulivi, C. Superoxide dismutases and their impact upon human health. *Mol. Asp. Med.* **26**, 340–352 (2005).

96. Calleja, L. F. et al. Activation of ALDH1A1 by omeprazole reduces cell oxidative stress damage. *FEBS J.* **288**, 4064–4080 (2021).

97. Sun, N. H. et al. A dose-response meta-analysis reveals an association between vitamin B12 and colorectal cancer risk. *Public Health Nutr.* **19**, 1446–1456 (2016).

98. Friso, S. & Choi, S.-W. The potential cocarcinogenic effect of vitamin B12 deficiency. *Clin. Chem. Lab. Med. (CCLM)* **43**, 1158–1163 (2005).

99. El-Sharkawy, A. & Malki, A. Vitamin D signaling in inflammation and cancer: Molecular mechanisms and therapeutic implications. *Molecules* **25**, 3219 (2020).

100. Rinninella, E., Mele, M. C., Raoul, P., Cintoni, M. & Gasbarrini, A. Vitamin D and colorectal cancer: Chemopreventive perspectives through the gut microbiota and the immune system. *Biofactors* **48**, 285–293 (2022).

101. Li, S. et al. Cholic Acid Stimulates MMP-9 in Human Colon Cancer Cells via Activation of MAPK, AP-1, and NF-κB Activity. *Int J Mol Sci* **21** https://doi.org/10.3390/ijms21103420 (2020).

102. Hu, J. et al. Lithocholic acid inhibits dendritic cell activation by reducing intracellular glutathione via TGR5 signaling. *Int. J. Biol. Sci.* **18**, 4545 (2022).

103. Ochsenkühn, T. et al. Colonic mucosal proliferation is related to serum deoxycholic acid levels. *Cancer* **85**, 1664–1669 (1999).

104. Cong, J. et al. Bile acids modified by the intestinal microbiota promote colorectal cancer growth by suppressing CD8+ T cell effector functions. *Immunity* (2024).

105. Jia, W., Xie, G. & Jia, W. Bile acid-microbiota crosstalk in gastrointestinal inflammation and carcinogenesis. *Nat. Rev. Gastroenterol. Hepatol.* **15**, 111–128 (2018).

106. Ma, Y. et al. Biosynthetic Pathway for Ethyl Butyrate Production in Saccharomyces cerevisiae. *J. Agric Food Chem.* **68**, 4252–4260 (2020).

107. Jan, G. et al. Propionibacteria induce apoptosis of colorectal carcinoma cells via short-chain fatty acids acting on mitochondria. *Cell Death Differ.* **9**, 179–188 (2002).

108. Park, J. S., Lee, E. J., Lee, J. C., Kim, W. K. & Kim, H. S. Anti-inflammatory effects of short chain fatty acids in IFN-gamma-stimulated RAW 264.7 murine macrophage cells: involvement of NF-kappaB and ERK signaling pathways. *Int Immunopharmacol.* **7**, 70–77 (2007).

109. Carretta, M. D., Quiroga, J., López, R., Hidalgo, M. A. & Burgos, R. A. Participation of short-chain fatty acids and their receptors in gut inflammation and colon cancer. *Front. Physiol.* **12**, 662739 (2021).

110. Wang, T. et al. Probiotics Lactobacillus reuteri Abrogates Immune Checkpoint Blockade-Associated Colitis by Inhibiting Group 3 Innate Lymphoid Cells. *Front Immunol.* **10**, 1235 (2019).

111. Li, R. et al. Expressing cytotoxic compounds in Escherichia coli Nissle 1917 for tumor-targeting therapy. *Res. Microbiol.* **170**, 74–79 (2019).

112. Matsuda, K. et al. Establishment of an analytical system for the human fecal microbiota, based on reverse transcription-quantitative PCR targeting of multicopy rRNA molecules. *Appl. Environ. Microbiol.* **75**, 1961–1969 (2009).

113. Geertsema, S. et al. Unsuitability of the Oxidation-Reduction Potential Measurement for the Quantification of Fecal Redox Status in Inflammatory Bowel Disease. *Biomedicines* **11**, 3107 (2023).

114. Bier, A. W. Introduction to oxidation reduction potential measurement. Hach Company, Lit (2009).

Acknowledgements

Author contributions

Tuoyu Zhou and Jingyuan Wu designed the study, performed experiment, prepared original daft and analyzed output date. Aman Khan and Yiqing Wang help to analyze date. Shaochen Su and El-Sayed Salama contributed to manuscript revisions and provide Methodology. Tianxiang Hu, Huawen Han and Weilin Jin contributed substantially to the revisions. Xiangkai Li also conceived the study and provided financial support and supervision. All the authors read and approved the final manuscript.

Competing interests

The authors declare no competing interests.

Additional information

Supplementary information The online version contains supplementary material available at https://doi.org/10.1038/s41538-024-00307-5.

Correspondence and requests for materials should be addressed to Huawen Han, Weilin Jin or Xiangkai Li.

Reprints and permissions information is available at http://www.nature.com/reprints

Publisher's note Springer Nature remains neutral with regard to jurisdictional claims in published maps and institutional affiliations.